Check for updates

Degradation of per- and polyfluoroalkyl substances (PFASs) by Fenton reactions

Zhicong Huang, [ID] Xi Huang, Kang Liu, [ID] Junwei Fu [ID] * and Min Liu [ID] *

Per- and polyfluoroalkyl substances (PFASs) are persistent organic pollutants with widespread environmental and health threats due to their chemical stability and bioaccumulative potential. The Fenton-based degradation of PFAS demonstrates several advantages, including mild reaction conditions, operational simplicity, and cost-effectiveness, while simultaneously facing challenges such as inefficient cleavage of carbon–fluorine (C–F) bonds and low mineralization. This review comprehensively summarizes the degradation of PFASs using Fenton-based reactions, focusing on mechanisms, efficiencies, and technological advancements. Firstly, the reasons for PFAS prevalence in human society, their pathways into biological systems, the associated health risks, as well as their global distribution and contamination status are elucidated. Secondly, the current major PFAS degradation approaches are summarized, highlighting the principal advantages of Fenton-based degradation. Thirdly, a comprehensive overview of recent advancements in Fenton-based PFAS degradation technologies is reviewed, including chemical-Fenton, electro-Fenton, photo-Fenton, and photo-electro-Fenton processes. Finally, the future research directions are discussed, focusing on catalyst design optimization, structure–activity relationship, and feasibility assessment for large-scale applications. This review provides a critical foundation for advancing sustainable PFAS remediation technologies.

Environmental significance

Per- and polyfluoroalkyl substances (PFASs) are synthetic chemicals widely used in industrial and consumer products due to their thermal and chemical stability. However, their resistance to environmental degradation, bioaccumulative behavior, and links to serious health effects have raised global concern. Traditional removal methods, such as adsorption and filtration, are limited by their inability to destroy PFASs, risking secondary pollution. Fenton-based advanced oxidation processes offer a promising pathway toward PFAS mineralization under mild conditions. This review provides a comprehensive analysis of the mechanisms, effectiveness, and technological progress of Fenton-based PFAS degradation. By highlighting current limitations and future directions, it aims to guide the development of practical, scalable, and sustainable remediation strategies for PFAS-contaminated environments, contributing to global efforts in safeguarding ecological and human health.

1. Introduction

Per- and polyfluoroalkyl substances (PFASs) comprise a class of over 6500 distinct anthropogenic fluorinated organic compounds,[1,2] characterized by fully or partially fluorinated alkyl chains, terminated with polar acidic moieties such as carboxylates, sulfonates, or phosphonates.[3] Based on the carbon-chain length, PFASs are generally classified into long-chain and short-chain types.[4] Long-chain PFASs, such as perfluorononanoic acid (PFNA) and perfluoropentanoic acid (PP), with more than eight carbon atoms, exhibit distinct physicochemical properties compared to short-chain PFASs (such as perfluorobutanesulfonic acid (PFBS), perfluorohexanoic acid (PFHxA), and perfluorohexanesulfonic acid (PFHxS), with four to seven carbon atoms). These differences are especially evident

in aqueous solubility and hydrophilicity, which can be quantified by solubility measurements and octanol–water partition coefficients.[5,6] For example, short-chain PFASs contain fewer fluorine atoms and lack the pronounced "molecular-brush" architecture of their long-chain counterparts,[1,2] thus having stronger water solubility and affinity for aqueous phases.[5] Beyond chain length, the inherent stability of PFASs stems from their abundant C–F bonds.[7] The high electronegativity of F atoms induces strong electron localization, thereby giving the C–F bonds extremely high polarity and bond energy ($\sim$110 kcal mol^{-1}).[8] The thermally and chemically robust C–F bonds endows PFASs with outstanding stability, unique lubricating and frictional characteristics, driving their extensive industrial applications since the 1940s, such as refrigerants, polymer-processing aids, pharmaceutical syntheses, adhesives, insecticides, and flame retardants (Fig. 1).[9,10]

PFASs were first detected in human serum in the 1960s,[11] which prompted studies on their environmental and biological

School of Physics, Central South University, Changsha 410083, People's Republic of China. E-mail: fujunwei@csu.edu.cn; minliu@csu.edu.cn

© 2026 The Author(s). Published by the Royal Society of Chemistry
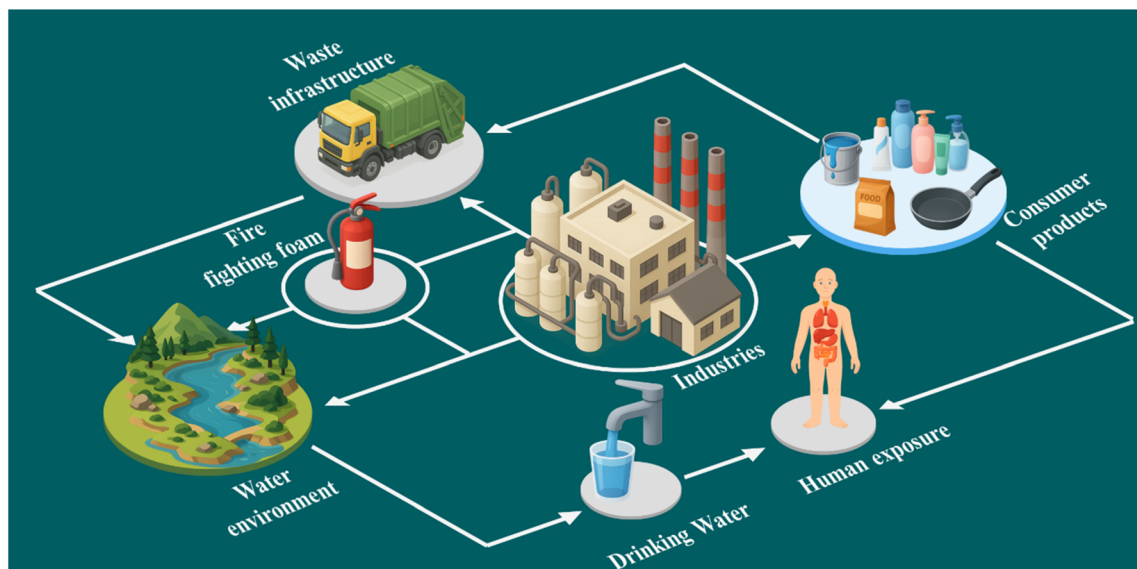
Environ. Sci.: Adv., 2026, 5, 9–42 | 9

Fig. 1   Migration process of PFASs in the environment.

risks. Their bioaccumulative potential is well established, with pronounced biomagnification in aquatic food webs.[12] Primary producers (*e.g.*, phytoplankton) capture PFASs and introduce them into ecosystems. For aquatic vertebrates (*e.g.*, *Cyprinus carpio* and *Danio rerio*), they directly absorb PFASs through gills, establishing trophic transfer pathways.[13] In particular, perfluoroalkyl phosphinic acids (PFPiAs) upregulate lipid transport genes (*e.g.*, *cd36* and *fabp1*), leading to hepatic steatosis. The disruption of β-oxidation and phospholipid metabolism induces reactive oxygen species (ROS), activates NF-κB, elevates pro-inflammatory cytokines (tnf-α, il-1β, and il-6), suppresses il-10,[14–17] and triggers inflammation. Perfluorooctane sulfonate (PFOS) analogues bind transthyretin, disturbing thyroid homeostasis.[18] In plants, PFASs are root-absorbed and transported to their above-ground parts. In wheat, fulvic and humic acids (HA) promote the uptake of 6 : 2 Cl-PFAES *via* H$^+$-ATPase and Ca^{2+}-dependent pathways.[19,20] In *Arabidopsis*, PFAS-induced

ROS causes lipid peroxidation and structural damage.[21–26] Structure-specific effects include PFOA-mediated cation disruption,[22] PFOS-induced amino acid dysregulation,[23] and 8 : 2 FTSA conversion impacting lipid metabolism.[26] In mammals, PFAS induce neuro-, hepato-, and reproductive toxicity, and worsen gut inflammation.[27,28] Dermal exposure models confirm systemic accumulation *via* CD36-mediated uptake, particularly in liver/kidneys.[29–31] Bioaccumulation is structure- and species-dependent, warranting further mechanistic research.

Due to the bioaccumulative potential and ecotoxicity of PFASs, their environmental contamination has become a pressing concern. Regulatory frameworks demonstrate increasing recognition of PFAS risks. In 2016, the U.S. Environmental Protection Agency (EPA) established health advisory levels at 0.070 μg L^{-1} for PFOS. Recent revisions have drastically reduced these thresholds to 0.004 ng L^{-1} for PFOA and 0.02 ng L^{-1} for PFOS.[32] The EU Water Framework Directive
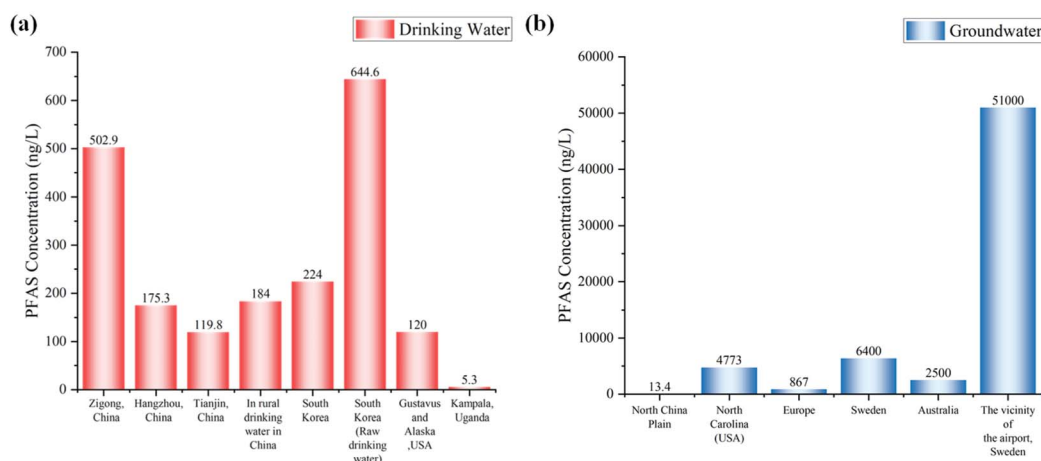

Fig. 2   The concentration of PFASs in different water sources: (a) drinking water and (b) groundwater.

10 | *Environ. Sci.: Adv.*, 2026, **5**, 9–42

© 2026 The Author(s). Published by the Royal Society of Chemistry

proposes a cumulative limit of 0.1 $\mu g\ L^{-1}$ for 20 prioritized PFAS compounds.[33] However, measured concentrations of PFASs in drinking water and groundwater worldwide often far exceed these thresholds (Fig. 2).
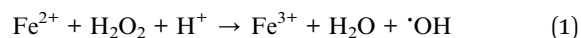
Drinking water surveys reveal widespread contamination, with most urban supplies containing >100 ng L^{-1} PFASs globally.[34–41] South Korea exhibits the highest concentrations (644.6 ng L^{-1}) in untreated drinking water (Fig. 2a),[38] attributable to dense clustering of chemical plants, electronics manufacturers, and textile facilities discharging PFAS-laden effluents. Conversely, Kampala, the capital of Uganda, shows minimal contamination (5.3 ng L^{-1}) (Fig. 2a),[41] potentially due to water sourcing from Murchison Bay, where lake dilution mitigates PFAS levels.

The groundwater system is more severely polluted, with the concentrations of PFASs in it being 25 to 500 times higher than in drinking water.[42–49] Extreme contamination occurs near Swedish airports (51 000 ng L^{-1}) (Fig. 2b),[47] exceeding EU standards by 510 times, and stemming from the unregulated release of PFAS-containing firefighting foam over several decades. A recent investigation in Shandong Province of China—home to one of Asia's largest fluorochemical industrial parks—identified severe PFAS discharge into nearby streams.[50,51] Although the affected waterways are relatively small, the industrial park's emissions—totaling 8.4 t of HFPOs (hexafluoropropylene oxides)—represent 85% of all HFPO discharges into rivers across China.[52] In contrast, North China Plain aquifers show relatively low PFAS levels (13.4 ng L^{-1}) (Fig. 2b),[42] correlating with limited industrial activity in the region. Recent reports indicate that PFAS concentrations in industrial wastewater treatment plants span a wide range, from 310 to 4920 ng L^{-1} in influents and from 246 to 27 100 ng L^{-1} in effluents, reflecting variations over several orders of magnitude.[53] The overall PFAS levels observed in these facilities are comparable to those recently reported in Korea for domestic wastewater (>1000 ng L^{-1}) and industrial wastewater (>5000 ng L^{-1}),[54] as well as in fluorochemical wastewater treatment plants in France (25 260 ng L^{-1}).[55] These cases highlight that industrial wastewater discharge is the primary PFAS entry route into ecosystems. The extreme environmental persistence of PFASs facilitates progressive accumulation, posing severe ecological threats. Consequently, extensive research now focuses on developing effective PFAS degradation technologies and remediation strategies.

2. Prevailing PFAS degradation strategies

A wide variety of purification methods for PFASs have been developed to date, including biodegradation approaches,[56,57] physical adsorption,[58,59] and chemical degradation (oxidation and reduction processes).[60–63] However, physical adsorption, being a non-destructive process, may generate secondary waste such as spent adsorbents, which pose a risk of re-releasing PFASs into the environment. In contrast, biodegradation and chemical degradation aim at the permanent removal of PFASs. Nevertheless, biodegradation is often incomplete, slow, and highly dependent

on specific environmental conditions.[64] More importantly, it is difficult to break the extremely strong C–F bonds of PFAS molecules. Among the chemical degradation methods, advanced oxidation processes (AOPs), first introduced by Glaze in 1987, are characterized by the generation of highly reactive radical species as oxidants, and are regarded as promising technologies with strong potential for the complete mineralization of PFASs.[65,66] Among AOPs, the Fenton reaction is one of the most classical and widely studied techniques. The Fenton reaction was first discovered in 1894 by the French scientist Henry J. Fenton, who observed that tartaric acid could be deactivated and oxidized in a ferrous ion (Fe^{2+})/hydrogen peroxide (H_2O_2) system at pH 2–3.[67] The key advantages of the Fenton process include its high oxidative performance and operational simplicity at ambient temperature and atmospheric pressure.[68,69] Moreover, its toxicity is relatively low because H_2O_2 ultimately decomposes into environmentally benign species such as water (H_2O) and oxygen (O_2).[70] Mechanistically, utilizing Fe^{2+} as a catalyst enables the continuous and stable decomposition of H_2O_2 to generate hydroxyl radicals ($^\cdot OH$) (shown in eqn (1) and (2)). These highly reactive hydroxyl radicals subsequently attack organic pollutants present in water, initiating a cascade of oxidation reactions that ultimately mineralize the contaminants into carbon dioxide (CO_2) and H_2O, thereby achieving water purification.[71,72]

$$Fe^{2+} + H_2O_2 + H^+ \rightarrow Fe^{3+} + H_2O + {}^\cdot OH \qquad (1)$$

$$Fe^{3+} + H_2O_2 \rightarrow Fe^{2+} + HO_2^\cdot + H^+ \qquad (2)$$

For the complete mineralization of PFASs, the degradation pathway begins with the initial activation of the molecule to generate perfluoroalkyl radicals ($^\cdot C_nF_{2n+1}$). These radicals then react with $^\cdot OH$ to form unstable perfluoroalcohol intermediates, which readily undergo elimination reactions to release hydrogen fluoride (HF). The resulting acyl fluoride intermediates are highly prone to hydrolysis, leading to the formation of shorter-chain perfluorocarboxylic acids.[73] Through successive cycles of similar reactions, PFOA can eventually be mineralized into CO_2 and HF (Fig. 3).[74,75] The ability of the Fenton system to continuously supply hydroxyl radicals makes it a promising approach for driving the deep oxidative degradation and potential mineralization of PFASs.

However, the Fenton reaction also exhibits certain limitations. When treating wastewater, its efficiency is influenced by factors such as pH and iron ion concentration of wastewater. Neither low nor high pH values enable effective treatment of organic pollutants. The optimal treatment efficiency is achieved within a pH range of 2.0–4.0.[76,77] Unfortunately, most organic wastewaters do not naturally fall within this pH range. Substantial amounts of chemical reagents are often required to adjust the pH prior to treatment, which increases the overall cost of wastewater remediation. Furthermore, while eqn (1) and (2) form the basis for the catalytic cycle of the Fenton reaction, the rate of reaction (1) is approximately 6000 times faster than that of reaction (2),[78] which severely hampers the regeneration of Fe^{2+} from Fe^{3+} and leads to the accumulation of Fe^{3+} in the system. When the pH values are above 3, Fe^{3+} tends to

© 2026 The Author(s). Published by the Royal Society of Chemistry

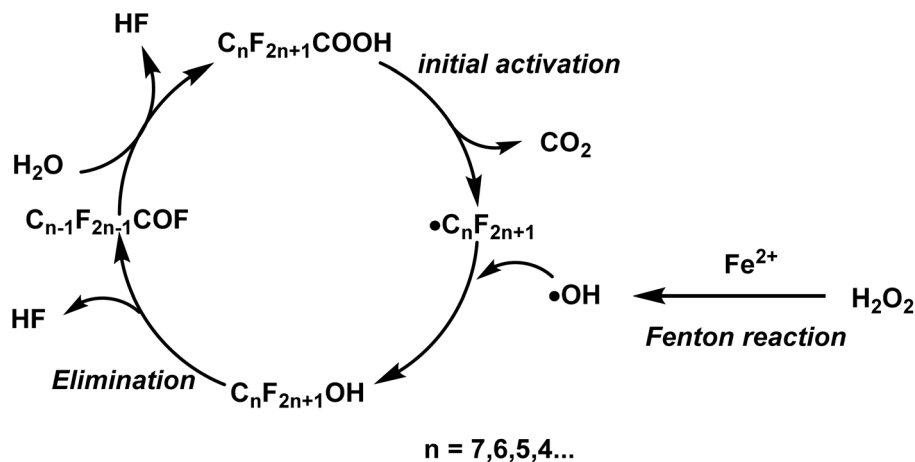*Environ. Sci.: Adv.*, 2026, **5**, 9–42 | 11

Fig. 3 Reaction mechanism for degradation of PFOA *via* the Fenton process. Upon completion of each reaction cycle, the value of *n* decreases by one, initiating the subsequent cycle.
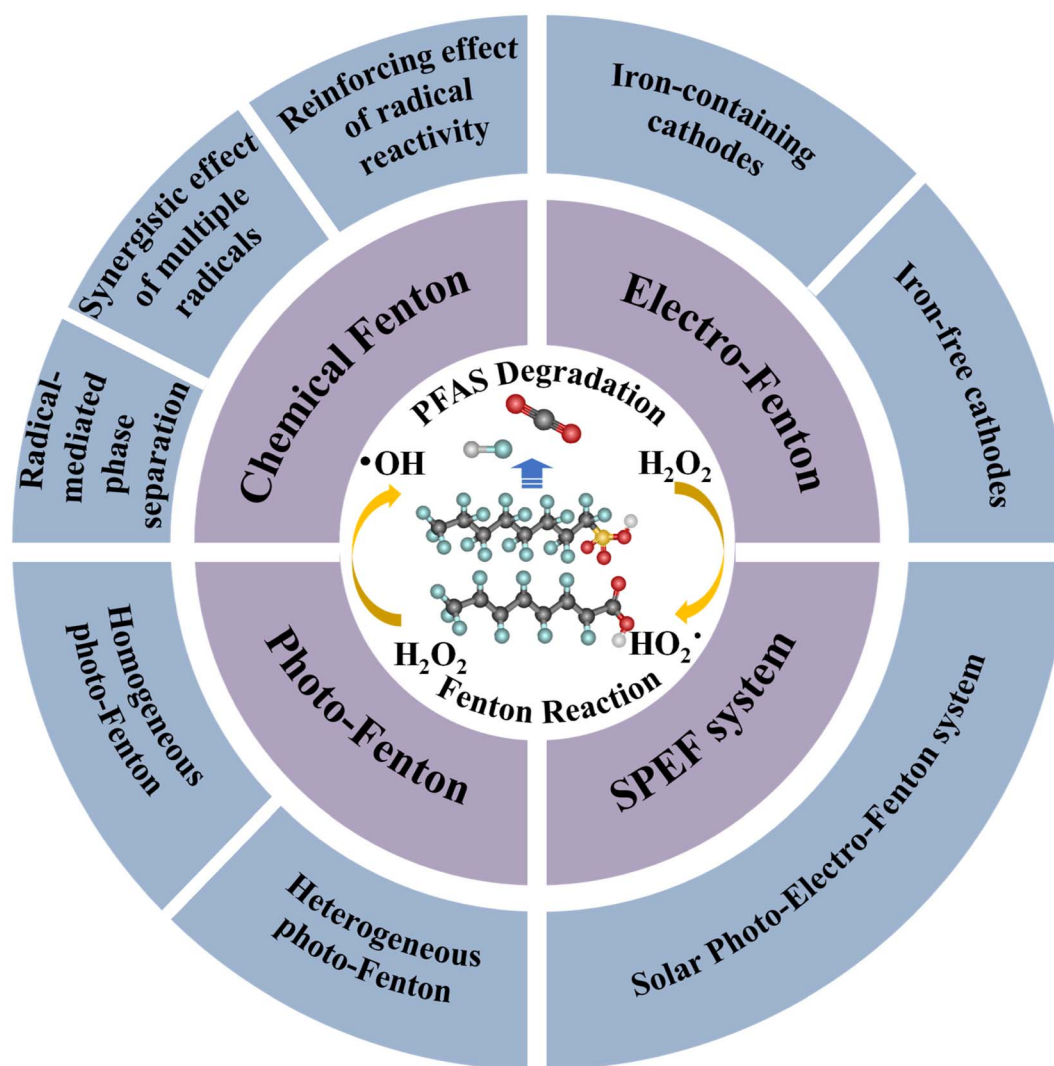

Fig. 4 Summary diagram of the contents in this review.

precipitate as hydroxide complexes—commonly referred to as iron sludge.[79] This sludge is difficult to separate and recover, resulting in substantial loss of catalytic iron species, reduced process efficiency, and the risk of secondary environmental pollution. To overcome these limitations, various strategies have been developed to enhance the Fenton reaction. Depending on the enhancement method, these approaches can be categorized into chemical-Fenton,[80–87] electro-Fenton,[88–93] UV/visible/solar light-assisted Fenton (photo-Fenton),[94–101] and solar photo-electro-Fenton (SPEF) systems.[102–107] Moreover, these technologies can be integrated in a synergistic or coupled manner to minimize or even eliminate the limitations associated with individual processes.

Herein, we focus on the research progress in utilizing Fenton reaction systems for PFAS degradation (Fig. 4). Through a systematic discussion of various Fenton systems, this review extensively elucidates degradation pathways, degradation efficiency, the redox potentials of different radical species, byproduct formation, and toxicity assessment. The primary objectives of this review are as follows: (1) to summarize the pathways and mechanisms of different Fenton reaction systems; (2) to summarize the degradation efficiencies of various radicals involved in PFAS removal under Fenton reaction conditions; (3) to systematically compare factors influencing PFAS degradation efficiency; (4) to summarize byproduct formation across different Fenton reaction systems and critically analyze their associated toxicity; and (5) to outline future research prospects. This review aims to establish a theoretical foundation for PFAS removal in practical applications.

3. Degradation of PFASs via Fenton reactions

3.1 Chemical-Fenton reaction system

Although the classical chemical Fenton reaction provides a stable and efficient source of $\cdot OH$, these radicals alone have proven inadequate for the effective degradation of PFASs. For instance, in the case of PFOA, studies have demonstrated that even under high concentrations of H_2O_2, the degradation efficiency is significantly low. Even with the addition of Fe^{2+} and H_2O_2, negligible degradation of PFOA and PFOS was observed, indicating the limited oxidative capacity of conventional $\cdot OH$-based systems in attacking the highly stable C–F bonds.[108,109] In response, considerable efforts have been made to expand and
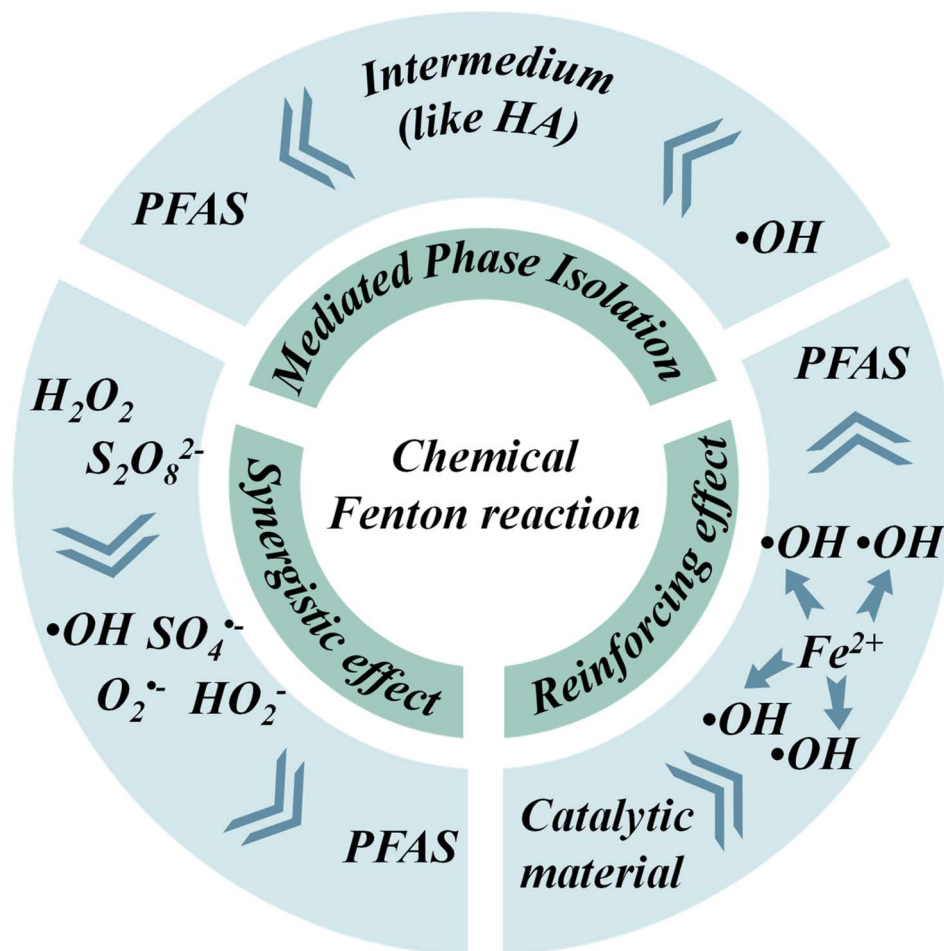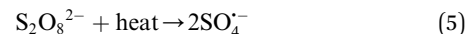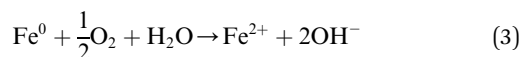

Fig. 5   Progress in the chemical Fenton reaction system toward PFAS remediation.

© 2026 The Author(s). Published by the Royal Society of Chemistry

Environ. Sci.: Adv., 2026, **5**, 9–42 | 13

modify chemical Fenton systems, employing diverse strategies to enhance the degradation efficiency of PFASs, such as the synergistic effect of multiple radicals, the reinforcing effect of radical reactivity, and radical-mediated phase separation (Fig. 5).

3.1.1 Synergistic effect of multiple radicals. To enhance the PFAS degradation ability of the chemical Fenton reaction system, the potential of multi-radical synergistic degradation was evaluated. Lo *et al.* developed a chemical Fenton reaction system employing zero-valent iron (ZVI) to activate persulfate (PS) and $^{\bullet}OH$ for the decomposition of perfluorooctanoic acid (PFOA).[80] In this system, PS acts as a sulfate radical ($SO_4^{\bullet-}$) precursor, while ZVI serves as a catalyst to lower the activation energy required for the generation of $SO_4^{\bullet-}$ (shown in eqn (3)–(6)). At the optimal temperature, the degradation rate of PFOA increased from 10% (using $^{\bullet}OH$ alone) to 68% with the combined action of $SO_4^{\bullet-}$ and $^{\bullet}OH$ (Fig. 6a), while the defluorination efficiency improved from 19% to 23% (Fig. 6b) within 2 hours, indicating a significant synergistic effect between $SO_4^{\bullet-}$ and $^{\bullet}OH$ radicals in promoting PFOA degradation. Notably, $SO_4^{\bullet-}$ has a higher redox potential of up to 2.6 V, exceeding that of $^{\bullet}OH$ (2.3 V). Moreover, $SO_4^{\bullet-}$ demonstrate superior performance in initiating the degradation of PFOA by facilitating the formation of perfluoroalkyl radicals (Fig. 6c).

$$Fe^0 + \frac{1}{2}O_2 + H_2O \rightarrow Fe^{2+} + 2OH^- \quad (3)$$

$$Fe^0 + 2H_2O \rightarrow Fe^{2+} + 2OH^- + H_2 \quad (4)$$

$$S_2O_8^{2-} + heat \rightarrow 2SO_4^{\bullet-} \quad (5)$$

$$Fe^{2+} + S_2O_8^{2-} \rightarrow Fe^{3+} + SO_4^{\bullet-} + SO_4^{2-} \quad (6)$$

In order to further expand the reactive species involved in multi-radical coupling, Watts *et al.* developed a $^{\bullet}OH$/superoxide ($O_2^{\bullet-}$)/hydroperoxide anion (HO_2^-)-based multi-radical system, enabling a stable and efficient chemical Fenton process for the degradation of PFOA.[81] Through catalyzed hydrogen peroxide (H_2O_2) propagation (CHP) reactions, H_2O_2 can be continuously decomposed to generate $O_2^{\bullet-}$ and HO_2^- (shown in eqn (7)–(9)). $O_2^{\bullet-}$ contributes to maintaining the continuity of the Fenton process by reducing Fe^{3+} to Fe^{2+}, while HO_2^- is generally regarded as a strong nucleophile, capable of attacking electron-deficient carbon atoms in PFOA, particularly those adjacent to the carboxyl group (*e.g.*, the α-carbon). This process facilitates C–F bond cleavage and thus promotes both degradation and defluorination (Fig. 7a).[110] The concentrations of H_2O_2 affect the types and concentrations of free radicals. The synergistic effect of multiple radicals ($^{\bullet}OH$, $O_2^{\bullet-}$, and HO_2^-) was supported by the optimal degradation efficiency exceeding 80% (Fig. 7b). One mol of PFOA molecules contains 15 mol F atoms; at a 1 M H_2O_2 concentration, the ratio of F^- ions to PFOA molecules is approximately 15, indicating complete defluorination and mineralization performance (Fig. 7c).

$$^{\bullet}OH + H_2O_2 \rightarrow HO_2^{\bullet} + H_2O \quad (7)$$
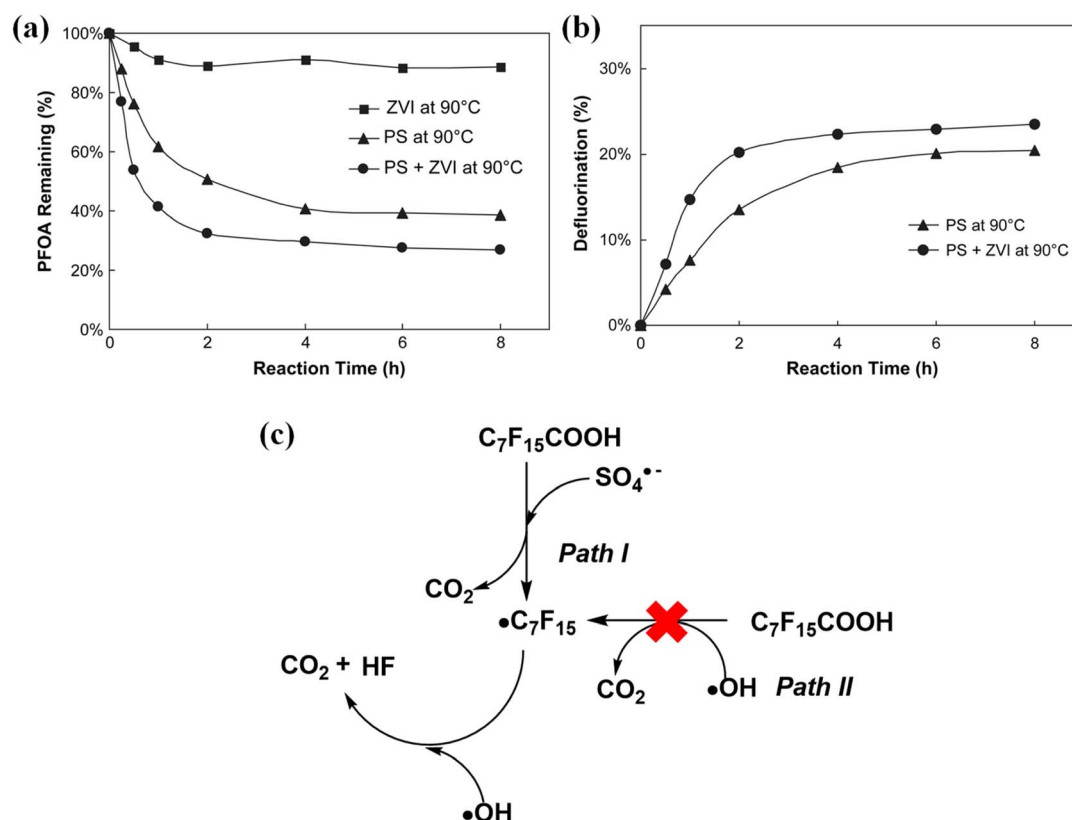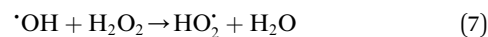

Fig. 6 (a) Comparison of the decomposition of PFOA in the presence of persulfate (PS) at 90 °C with or without ZVI. (b) The defluorination of PFOA with persulfate at 90 °C.[80] (c) The proposed synergistic mechanism of $^{\bullet}OH$ and $SO_4^{\bullet-}$ for PFAS degradation.
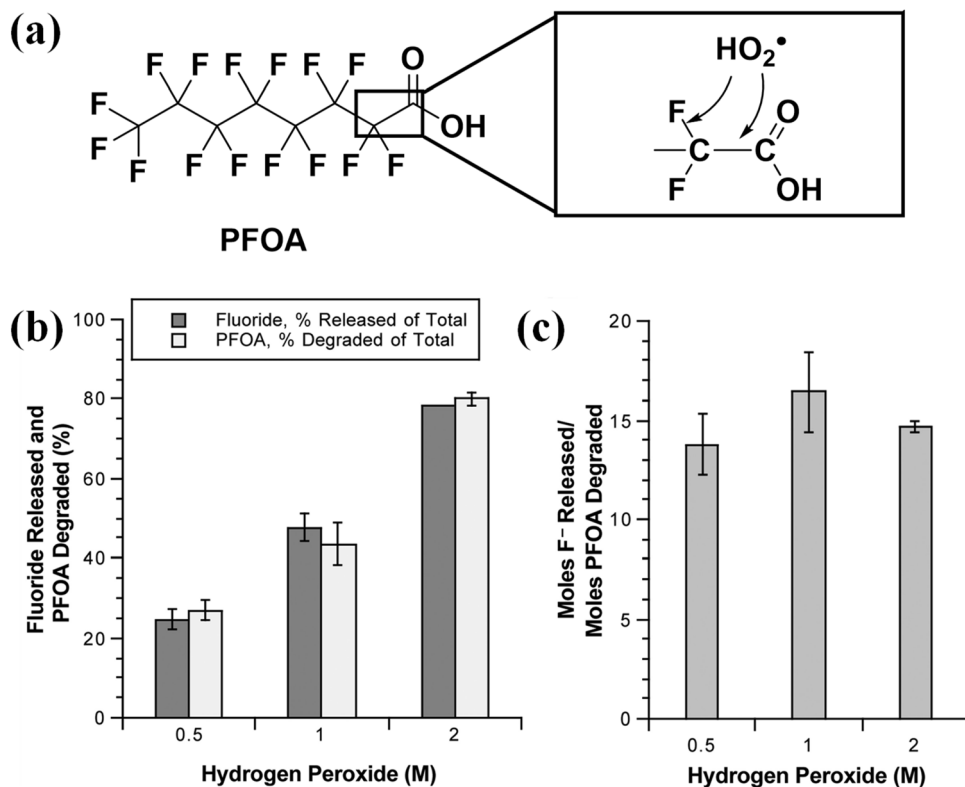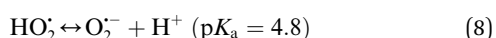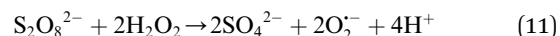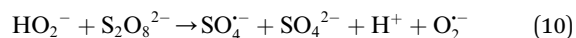
Fig. 7   (a) A schematic diagram of $HO_2^•$ radicals attacking electron-deficient carbon atoms in PFOA. (b) The defluorination and degradation efficiency of PFOA under different concentrations of hydrogen peroxide. (c) The ratio of moles of fluoride released to moles of PFOA degraded under different concentrations of hydrogen peroxide.[81]

$$HO_2^• \leftrightarrow O_2^{•-} + H^+ \ (pK_a = 4.8) \tag{8}$$

$$HO_2^• + Fe^{2+} \rightarrow Fe^{3+} + HO_2^- \tag{9}$$

In addition, the combination of $SO_4^{•-}$, $^•OH$, and $O_2^{•-}$ radicals has also proven effective. Choi et al. developed an iron-modified diatomite (MD) catalyst capable of efficiently generating $SO_4^{•-}$, $^•OH$, and $O_2^{•-}$, thereby promoting PFOA degradation through synergistic radical interactions.[82] The key advantage of the MD catalyst lies in its naturally abundant and low-cost material, as a stable and easily separable support for iron loading. At the same time, its high surface area is conducive to the generation of free radicals and the adsorption of pollutants. This system utilizes the catalytic ability of Fe^{2+} to activate H_2O_2 and PS, and can continuously and stably generate $^•OH$, $O_2^{•-}$ and $SO_4^{•-}$ (shown in eqn (1), (10) and (11)). In conventional dual-radical systems such as $^•OH/SO_4^{•-}$, the cleavage of highly inert C–F bonds in PFOA remains limited. However, the introduction of $O_2^{•-}$ induces an additional reductive and nucleophilic pathway targeting electron-deficient α-carbon atoms adjacent to the carboxyl group, thereby enhancing C–F bond cleavage (Fig. 8a). Moreover, the combination of $SO_4^{•-}$ (a strong oxidant 2.6 V) and $O_2^{•-}$ (a moderate reductant −0.33 V) provides a more diverse redox environment for Fe^{2+}/Fe^{3+} that improves the overall degradation efficiency. As experiment demonstrated, MD was capable of catalyzing both the Fenton reaction with H_2O_2 and

the CHP reaction, achieving a moderate PFOA degradation efficiency of 60% (Fig. 8b). When PS was further introduced into the reaction system, the synergistic effect of $SO_4^{•-}$, $^•OH$, and $O_2^{•-}$ radicals enhanced the degradation efficiency to 69% (Fig. 8c), highlighting the effectiveness of multi-radical cooperation.

$$HO_2^- + S_2O_8^{2-} \rightarrow SO_4^{•-} + SO_4^{2-} + H^+ + O_2^{•-} \tag{10}$$

$$S_2O_8^{2-} + 2H_2O_2 \rightarrow 2SO_4^{2-} + 2O_2^{•-} + 4H^+ \tag{11}$$

In summary, the development of multi-radical synergistic degradation strategies within Fenton-based systems has shown significant promise for improving PFAS treatment efficiency. The combined action of various reactive species—such as $^•OH$, $SO_4^{•-}$, $O_2^{•-}$, and $HO_2^•$—can substantially enhance the degradation process. This improvement is primarily attributed to: (1) the stronger oxidative potential of $SO_4^{•-}$, which can overcome the limitations of $^•OH$ in initiating the activation of PFAS molecules; (2) the presence of a multi-radical environment that increases the probability and efficiency of radical attacks on PFAS compared to systems dominated by a single radical species. However, multi-radical Fenton systems also face several limitations. The complexity of the reaction environment makes it difficult to clearly elucidate the underlying mechanisms and pathways of radical synergy. In addition, the overall degradation efficiency remains insufficient to meet the demands of rapid
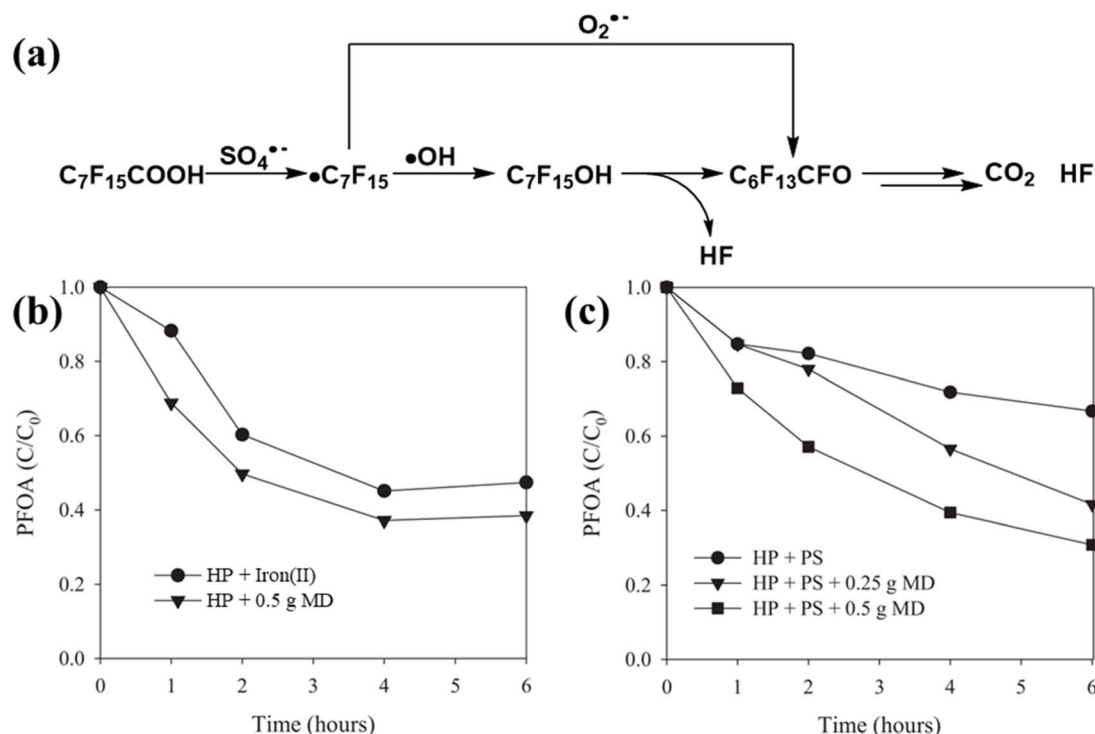
Fig. 8 (a) The PFOA degradation mechanism of $^{\bullet}OH$, $O_2^{\bullet-}$ and $SO_4^{\bullet-}$ radicals. (b) Decomposition of PFOA by catalyzed hydrogen peroxide propagation (CHP) reactions in the presence of dissolved Fe ions and in the presence of MD containing Fe species. (c) Decomposition of PFOA by different HP-activated PS systems.[82] HP: hydrogen peroxide, H_2O_2; PS: persulfate, $S_2O_8^{2-}$.

and effective PFAS removal. Therefore, efforts are being made to develop strategies aimed at further enhancing the radical reactivity.

3.1.2 Reinforcing effect of radical reactivity. To enhance the activity of reactive radicals, researchers have focused on material structural design with high specific surface areas, whose unique architectures provide several key advantages: (1) increased number of exposed Fe active sites, particularly on surfaces and within micropores; (2) limited diffusion pathways of PFAS molecules, enhancing the contact between contaminants and catalytic sites; and (3) confined microenvironments promoted the local accumulation and prolonged lifetime of reactive radicals.

Wang et al. fabricated a composite material by anchoring Pb-doped BiFeO₃ (Pb-BFO) nanoparticles onto reduced graphene oxide (rGO) nanosheets,[83] forming a layered architecture. The Pb-BFO nanoparticles were firmly immobilized on the rGO surface, which effectively inhibited nanoparticle agglomeration and preserved high surface reactivity. Moreover, the formation of nanoscale interlayer gaps between rGO sheets facilitated rapid electron transfer, thereby enabling the localized enrichment of $^{\bullet}OH$ within the confined interlayer space and the oxidative interaction between $^{\bullet}OH$ and PFAS molecules (Fig. 9a and b). Additionally, Pb doping improved the intrinsic charge transport properties of BFO, while the oxygen-containing functional groups (e.g., carboxyl and hydroxyl groups) of rGO were capable of activating H_2O_2 to produce $^{\bullet}OH$ radicals, collectively contributing to the improved catalytic efficiency of

the composite system (Fig. 9c). This approach achieved over 95% degradation efficiency of PFOA within 5 minutes, with nearly half of the PFOA undergoing complete mineralization (Fig. 9d). These results underscore the feasibility of employing porous materials to promote chemical Fenton-based degradation of PFASs.

For the purpose of further understanding the influence of the material structure on the efficiency of chemical Fenton degradation of PFASs, Shi et al. extended the structure of conventional two-dimensional reduced graphene oxide (rGO) into a three-dimensional graphene-based framework (OG),[84] in which the abundant C–O–C bridging structures were found to significantly enhance the Fenton reaction by promoting the generation efficiency of $^{\bullet}OH$ (Fig. 10a). Notably, the OG material was derived from recycled biomass waste, aligning with the principles of green chemistry and offering promising advantages in terms of environmental sustainability and economic viability. Density functional theory (DFT) calculations indicated that the C–O–C bridging structure of OG was key to electron transport. Electrons from the C–F bonds in PFOA could transfer to the OG surface via these bridges (Fig. 10b), with the F atom's HOMO contribution increasing significantly from 0.95% to 15.46% (Fig. 10c). Moreover, the spatial confinement effect of OG reduced the activation energy for H_2O_2 decomposition (1.10 eV for OG vs. 1.60 eV for 2D graphene).

Similar to the above strategy, Zhuang et al. synthesized an Fe/S co-doped carbon aerogel (PGFe),[85] in which sulfur doping played a crucial role in facilitating covalent bonding between
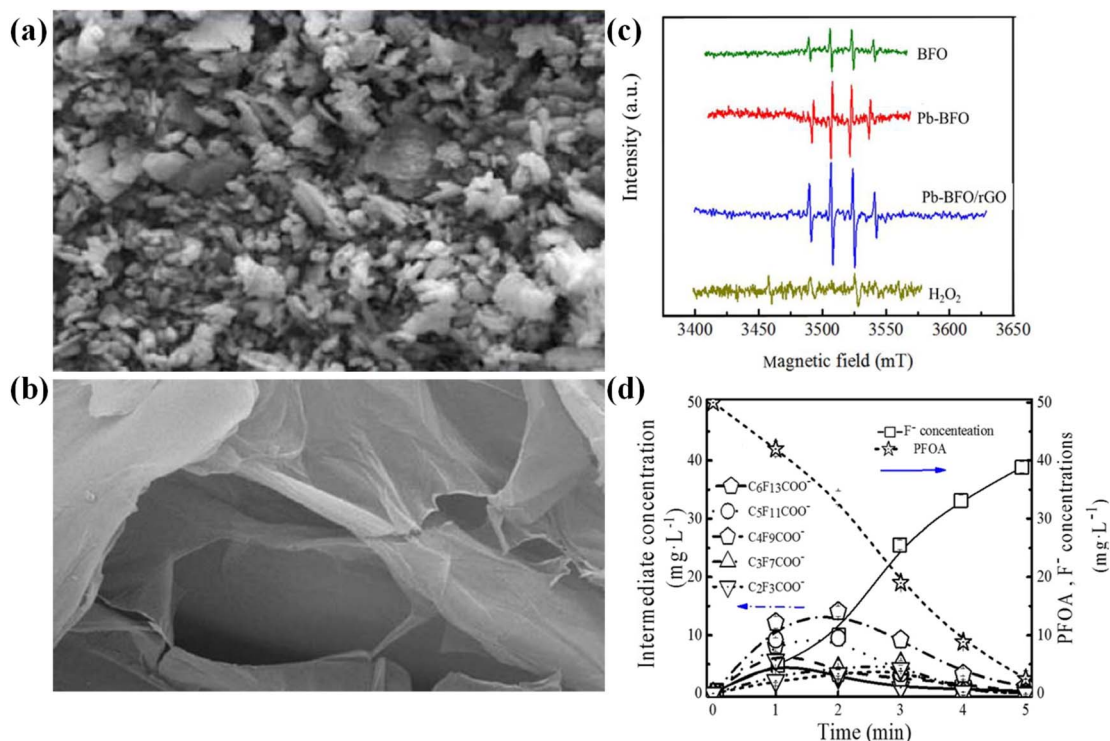
Fig. 9 SEM images of Pb-BFO/rGO (a) and GO (b) composites. (c) The EPR spectra of different catalyst suspensions. (d) Evolution of F⁻ concentration and degradation byproducts as a function of degradation time with the Pb-BFO/rGO system.[83]
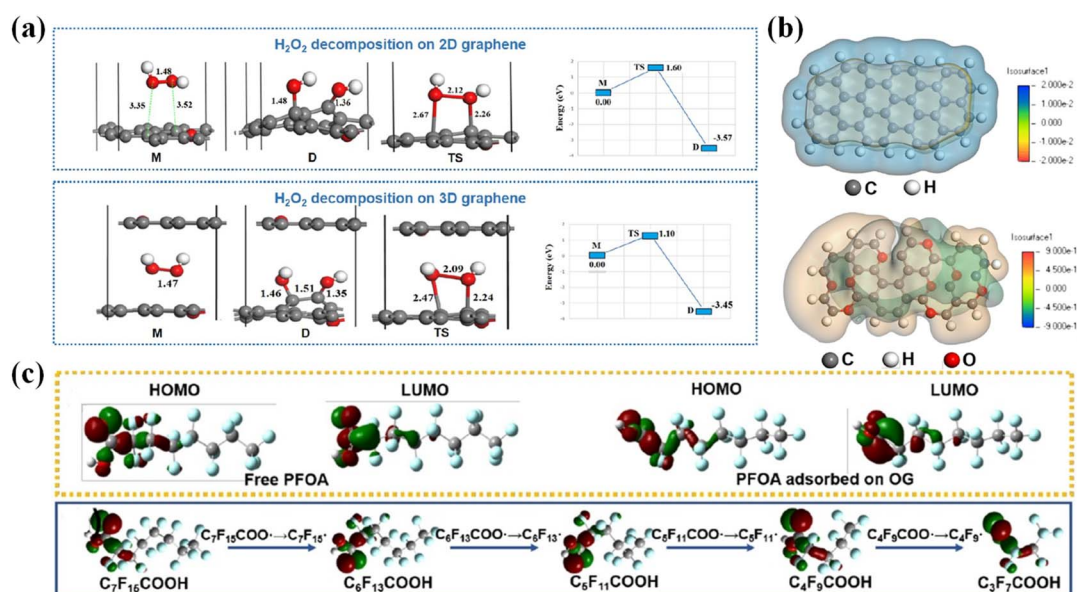
Fig. 10 (a) Energy profiles of H_2O_2 decomposition on 2D and 3D graphene. (b) Comparison of the electrostatic potential distributions of porous graphene and modified graphene. (c) HOMO and LUMO energies of free PFOA, PFOA adsorbed on OG and PFOA intermediates during degradation.[84]

iron and carbon, thereby enhancing the electronic conductivity of the material and accelerating the Fenton reaction by creating a more stable environment for ˙OH generation. Additionally, the incorporation of polyvinyl alcohol during the carbonization process promoted the formation of a highly porous structure, effectively increasing the specific surface area and exposing a greater number of active sites. Charge and electrophilicity analyses identified C7, C8, terminal F23, and electron-rich O24 atoms in the PFAS molecule as the most susceptible to ˙OH attack (Fig. 11a), providing a theoretical basis for predicting

© 2026 The Author(s). Published by the Royal Society of Chemistry

Environ. Sci.: Adv., 2026, 5, 9–42 | 17
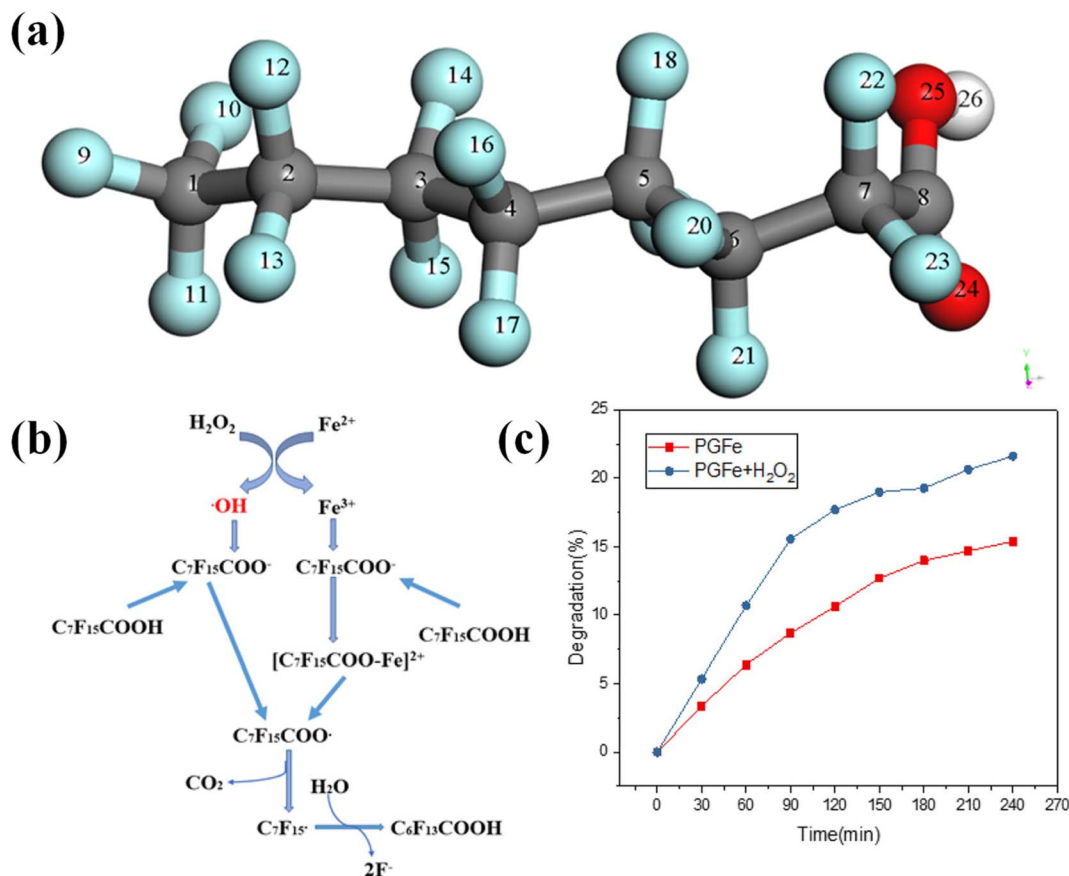
Fig. 11 (a) Structure of PFOA denoted by sequence numbers: 1–8 carbon, 9–23 fluorine, 24–25 oxygen and 26 hydrogen. (b) Schematic diagram of the degradation process of PFOA in the PGFe/H_2O_2 Fenton system. (c) PFOA degradation rate in PGFe and PGFe/H_2O_2 systems.[85]
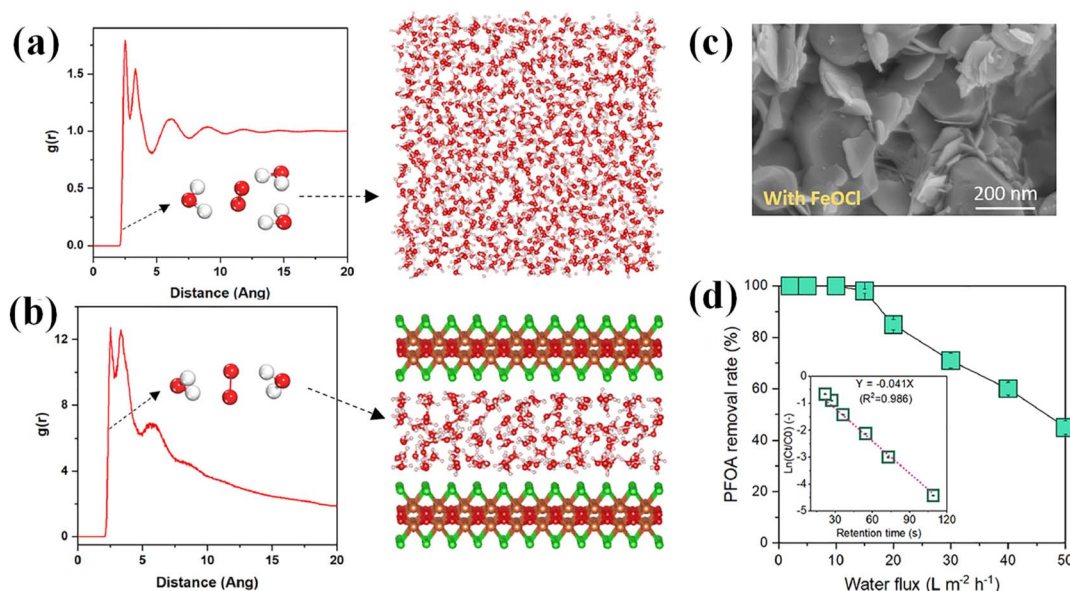
Fig. 12 (a) The RDF as a function of distance from free $O_2^{\bullet-}$ radicals and a snapshot of the free $O_2^{\bullet-}$ radicals in the aqueous phase. (b) The RDF as a function of distance from confined $O_2^{\bullet-}$ radicals and a snapshot of the $O_2^{\bullet-}$ radicals confined inside the FeOCl structure. (c) Cross-sectional SEM images of the FeOCl-incorporated ceramic membrane. (d) Fast degradation of PFOA through a heterogeneous Fenton reaction inside the FeOCl membrane.[86]

18 | Environ. Sci.: Adv., 2026, 5, 9–42

© 2026 The Author(s). Published by the Royal Society of Chemistry

bond cleavage pathways (Fig. 11b). This study provides a solid theoretical foundation for understanding the PFOA degradation process. The PFAS degradation efficiency *via* PGFe modified chemical Fenton-based reactions improved from 15% to 22% (Fig. 11c).

To further investigate the relationship between material porosity and the degradation rate of PFAS, Zhang *et al.* developed a layered iron oxychloride (FeOCl) catalyst.[86] By confining reactive species within a sub-nanometer spatial domain, the hydration coordination number of $O_2^{\cdot-}$ radicals generated from the Fenton reaction was modulated, reducing the average coordination number from 3.3 to 1.89 (Fig. 12a and b). The decreased coordination number concentrated the negative charge on $O_2^{\cdot-}$, strengthening its interaction with PFAS molecules. To further enhance spatial effect, FeOCl was immobilized onto ceramic membranes, the active channels were confined within a 20 nm scale (Fig. 12c). As a result, the apparent reaction rate constant (k_{obs}) reached 1.2 min^{-1} (Fig. 12d), which was 86 times higher than that of a traditional batch-mode system (0.014 min^{-1}). This study quantitatively demonstrated the performance enhancement of PFAS degradation reactions achieved by the confinement effect of high specific surface area materials and provides a feasible approach for future investigations into the structure–activity relationship for PFAS degradation.

Although structural design of materials can effectively enhance the interaction between reactive radicals and PFAS, numerous unresolved issues remain—such as how the sensitivity of spatial confinement to material dimensions influences radical reactivity, and whether atomic-level features within the catalyst structure affect the confinement effect. Additionally, the deep defluorination remains a challenge, especially for the degradation by-products of short chains.

3.1.3 Radical-mediated phase separation. To address the deep defluorination of PFAS and the accumulation of short-chain byproducts, Santos employed the abundant $\cdot$OH generated in the Fenton reaction system to oxidatively modify humic acid (HA) for phase separation of aqueous PFAS and their short-chain byproducts.[87] The HA molecules contain various functional groups, such as carboxyl and phenolic hydroxyl groups, which may be oxidized or rearranged during the reaction, resulting in the formation of new chemical bonds and larger structural assemblies. Through the oxidative transformation and restructuring of functional groups on HA, the interaction between HA and PFOA was enhanced, ultimately facilitating the transfer of PFOA from the aqueous phase to the solid phase *via* a co-precipitation and phase separation mechanism (Fig. 13a).

As the structure of HA evolves, it may form larger polymeric or network-like aggregates. These aggregates can physically entrap PFOA molecules adsorbed on their surfaces, effectively encapsulating them within the HA matrix (Fig. 13b). This encapsulation hinders the re-release of PFOA into the aqueous phase, thereby facilitating its removal from water. However, this process does not involve the chemical degradation of PFOA; rather, the molecule merely transfers from the aqueous phase to the solid phase. Consequently, the development of effective strategies for the removal of PFAS immobilized in solid phases has emerged as a critical focus area. Materials such as graphene, metal–organic frameworks (MOFs), and covalent organic frameworks (COFs) are being explored as advanced platforms capable of adsorbing PFASs and enabling their subsequent solid-phase separation under catalytic or advanced oxidation conditions.[111]

Substantial progress has been made in understanding the application of chemical-Fenton reactions for PFAS treatment. The chemical-Fenton system offers several advantages, including relatively simple experimental conditions, high selectivity, the synergistic action among multiple reactive radicals, and efficient PFAS degradation achieved through material structure designs. However, several limitations remain. (1) The requirement for high concentrations of H_2O_2 (≥ 1 M) not only leads to excessive reagent consumption but also poses significant safety concerns. (2) The system generally exhibits limited capacity to sustain the Fe^{2+}/Fe^{3+} redox cycle, raising challenges for maintaining long-term Fenton reactivity. (3) Like conventional Fenton systems, chemical Fenton processes have not overcome the inherent pH constraint, typically requiring pre-
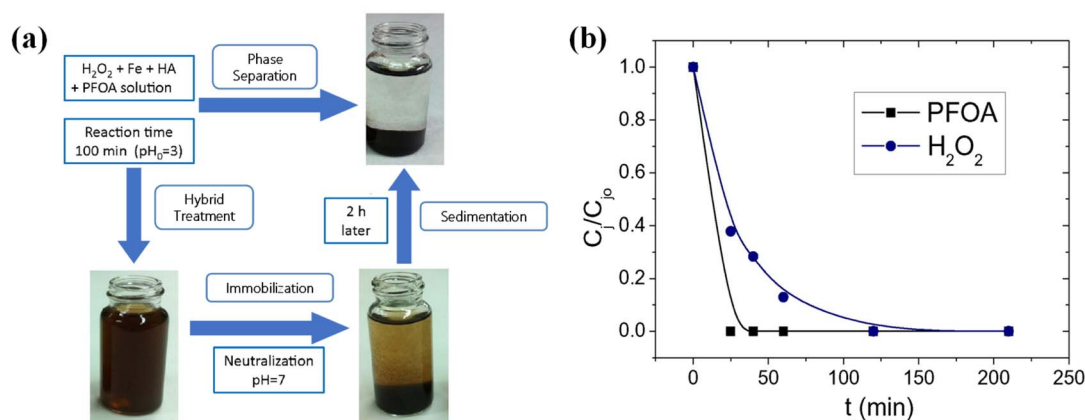

Fig. 13 (a) Illustration of the HA-coupled Fenton reaction driving multiphase conversion of PFOA. (b) Residual PFOA and oxidant in hybrid treatment of PFOA solution with Fenton-like reagent and humic acid.[87]

© 2026 The Author(s). Published by the Royal Society of Chemistry

Environ. Sci.: Adv., 2026, **5**, 9–42 | 19

acidification of the aqueous environment, which further restricts their practical applications.

3.2 Electro-Fenton reaction systems

The electro-Fenton (EF) process differs from the conventional chemical-Fenton reaction in mechanism. Efficient PFAS mineralization typically requires the initial activation of PFAS molecules into perfluoroalkyl radicals. In the chemical Fenton process, the generation of ˙OH alone is often insufficient; therefore, additional more potent oxidation species are needed to achieve effective degradation. In contrast, electro-Fenton systems utilize electrocatalysis—one of the most powerful redox techniques—to directly oxidize PFASs and form perfluoroalkyl radicals, thereby promoting further ˙OH generation and overall degradation efficiency. Moreover, the electro-Fenton process offers two additional advantages for PFAS remediation: (1) *in situ* generation of H_2O_2 *via* the oxygen reduction reaction (ORR), reducing reliance on external H_2O_2 dosing; and (2) improved Fe^{2+}/Fe^{3+} redox cycling under optimized electrochemical conditions, minimizing the formation of iron sludge (Fig. 14).

The electro-Fenton reaction represents a synergistic integration of chemical-Fenton and electrochemical methods. The anodes used in electro-Fenton systems are commonly boron-doped diamond (BDD) or Magnéli phase titanium suboxides (Ti_4O_7), similar to those in conventional electrochemical oxidation processes. These non-active anode materials are favored due to the following characteristics: (1) high chemical stability and inertness, conferring long operational lifespans;[112,113] (2) wide potential windows and high oxygen evolution potentials (>2.7 V *vs.* NHE), conducive to the cleavage of

C–F bonds;[114,115] and (3) excellent corrosion resistance, enabling compatibility with strong acidic or basic environments.[116]

The anode materials used in electro-Fenton systems are relatively fixed; ongoing research focuses on developing efficient cathode materials to enhance ORR performance for H_2O_2 generation. In this review, the electro-Fenton systems are categorized based on the cathode materials: iron-containing cathodes and iron-free cathodes.

3.2.1 Iron-containing cathodes. To evaluate the feasibility of a synergistic electro-catalytic system integrating cathodic electro-Fenton and anodic oxidation for effective PFOA removal, Zhao *et al.* synthesized an Fe–Mn co-doped carbon aerogel material (Fe10MnC). In this system, PFOA was initially activated at the anode, while the cathode facilitated the electro-Fenton reaction to efficiently generate ˙OH radicals (Fig. 15a). Through the strategic combination of these processes, an effective approach for the synergistic degradation of PFASs was developed.[88] BDD was employed as the anode material, capable of generating ˙OH (H_2O oxidation) with high efficiency. These radicals, alongside direct anodic oxidation, contributed to the cleavage of C–F bonds in PFOA (Fig. 15b). Meanwhile, Fe10MnC acted as the cathode, enabling the *in situ* electro-generation of H_2O_2 by the ORR, which was subsequently activated to produce ˙OH under the catalytic effect of Fe and Mn (Fig. 15c). Surface valence analysis revealed that Mn improved the selectivity for the two-electron ORR for H_2O_2 production (Fig. 15d). This system achieved a 97% PFOA removal rate within 4 hours of electrolysis, without hydrogen peroxide added and no iron sludge produced.

For the purpose of further expanding the range of reactive radicals in electro-Fenton processes, Cai *et al.* developed an
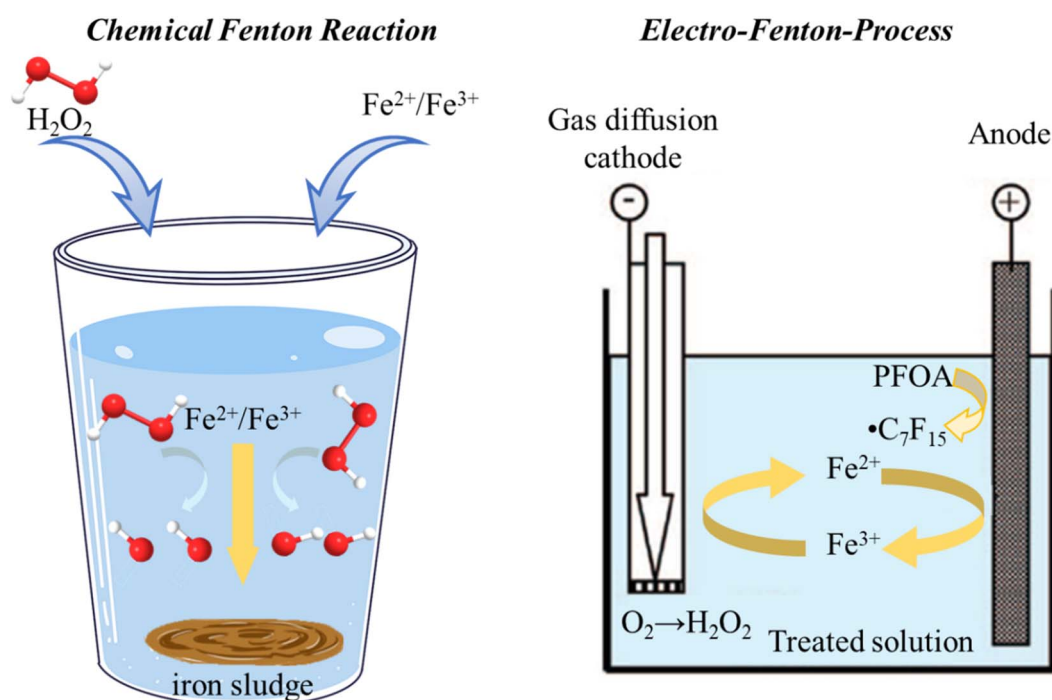
Fig. 14 Comparison between the chemical-Fenton reaction and the electro-Fenton process.
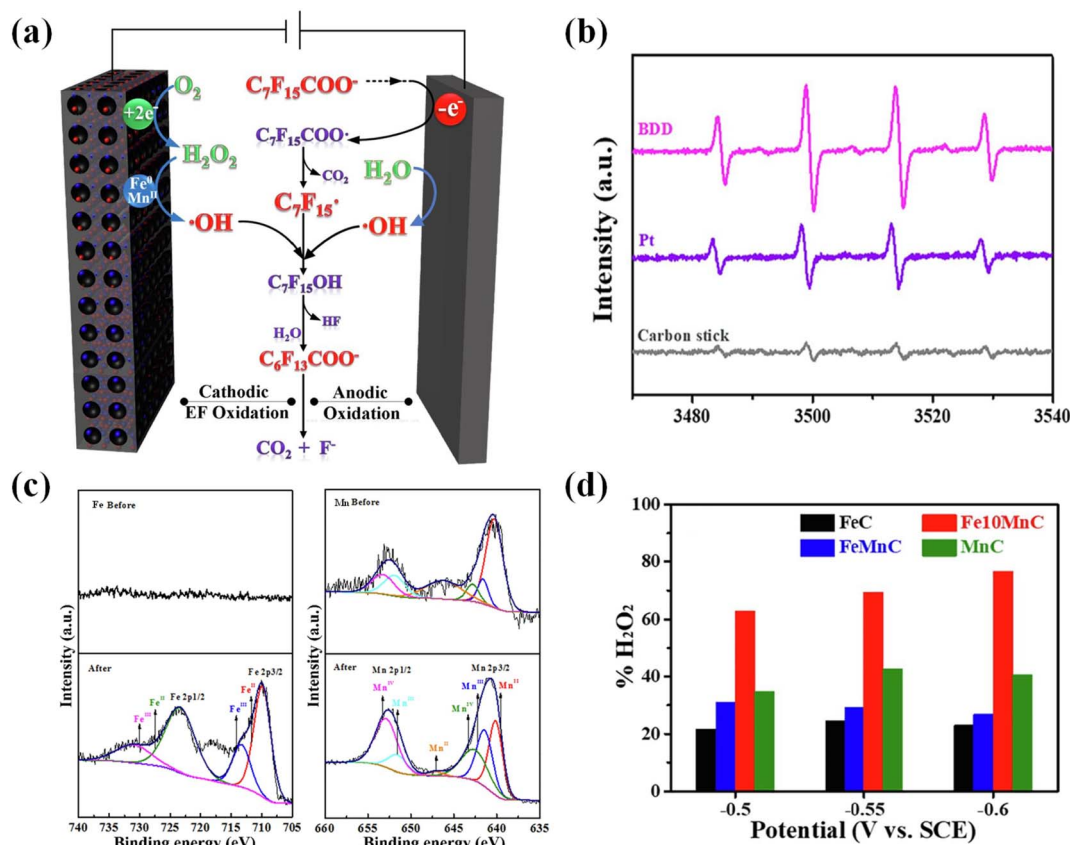
Fig. 15 (a) Catalytic mechanism of electro-Fenton oxidation for efficiently removing PFOA with Fe10MnC as the cathode and BDD as the anode. (b) EPR spectra of DMPO·OH adducts with different anodes. (c) Fe and Mn XPS spectra of Fe10MnC before and after PFOA degradation. (d) Productivity for H_2O_2 of different cathodes.[88]
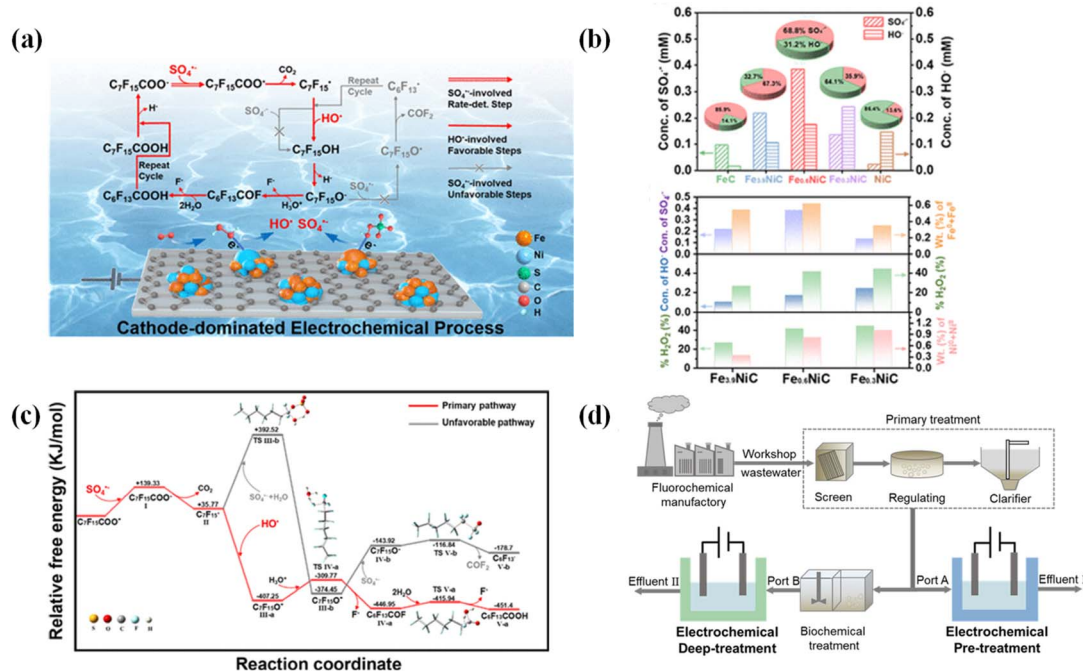
Fig. 16 (a) Schematic of PFOA degradation in a cathode-dominated electro-Fenton process. (b) The quantitative and cumulative concentration of $SO_4^{·-}$ and ·OH in different cathodes. (c) Profile of the potential energy surfaces for the PFOA degradation dominated by $SO_4^{·-}$ and ·OH. (d) Flowchart of fluorochemical manufactory wastewater treatment.[89]

iron–nickel co-doped carbon aerogel (Fe$_x$NiC), which enabled the coupling of SO$_4^{\cdot-}$ and $\cdot$OH radicals for effective PFOA degradation (Fig. 16a).[89] Unlike previous studies, a graphite electrode was employed as the anode, which minimized anodic oxidation of PFOA and thus better highlighted the superior performance of the cathodic material in the degradation process. By adjusting the Fe/Ni ratio, the generation rates of SO$_4^{\cdot-}$ and $\cdot$OH radicals can be modulated (Fig. 16b). While iron is essential for Fenton chemistry, it tends to favor the four-electron reduction pathway in the ORR, producing H$_2$O instead of H$_2$O$_2$.[117] Ni doping enhanced the selectivity toward the two-electron pathway, promoting efficient H$_2$O$_2$ generation. DFT calculations supported a synergistic degradation mechanism involving SO$_4^{\cdot-}$ and $\cdot$OH: initially, SO$_4^{\cdot-}$ attacks the carboxylic group of PFOA, forming the carboxyl radical C$_7$F$_{15}$COO$^\cdot$ (ΔG = 139.33 kJ mol^{-1}), which undergoes decarboxylation to form the perfluoroalkyl radical C$_7$F$_{15}^\cdot$ (ΔG = −103.56 kJ mol^{-1}). This radical then reacts with $\cdot$OH to yield perfluorinated alcohol C$_7$F$_{15}$OH (ΔG = −443.02 kJ mol^{-1}), which undergoes HF elimination (ΔG = 97.48 kJ mol^{-1}) and hydrolysis (Fig. 16c), leading to stepwise chain shortening and eventual complete mineralization.

In real wastewater treatment scenarios (Fig. 16d), for raw effluent from a fluorochemical plant in Sichuan (PFOA = 8.69 mg L^{-1}), electro-Fenton treatment achieved promising performance after biochemical treatment, with 81% degradation and 52% defluorination within 4 h (Effluent II). Even for raw wastewater without biochemical pretreatment, comparable results were obtained under the same conditions, with 75% degradation and 58% defluorination after 4 h (Effluent I), clearly demonstrating the application potential of this method. In terms of chemical oxygen demand (COD) reduction, the process was likewise effective: for Effluent II, COD decreased from 47.7 mg L^{-1} to 26.4 mg L^{-1}, while for Effluent I, COD was reduced from 1060 mg L^{-1} to 540 mg L^{-1}, meeting the Chinese Surface Water Quality Standard (GB3838-2002). Notably, the energy consumption for the treatment of Effluents I and II was approximately 0.39 and 0.018 kWh g^{-1}, respectively, further underscoring the viability of this approach for industrial applications.

In order to highlight the positive contribution of cathodic electro-Fenton reactions for effective degradation of PFOA, Han *et al.* synthesized a bifunctional single-atom catalyst with a Co-CN$_2$ configuration supported on an Fe$_2$O$_3$ substrate (Co-CN$_2$-Fe$_2$O$_3$) (Fig. 17a).[90] The critical role of the cathode in enhancing the generation of reactive oxygen species and improving overall system performance was investigated. A platinum anode was used to eliminate contributions from anodic oxidation, enabling a focused assessment of cathodic degradation. In this system, the Co-CN$_2$ single-atom layer facilitated the two-electron ORR for efficient H$_2$O$_2$ generation (Fig. 17b and c). The low-coordination Co sites in the Co-CN$_2$ structure weakened O$_2$ adsorption and prevented O–O bond cleavage, thereby improving H$_2$O$_2$ selectivity. The Fe$_2$O$_3$ substrate functioned as the Fenton catalyst to activate the *in situ* generated H$_2$O$_2$ into $\cdot$OH. This system achieved 96% PFOA degradation (Fig. 17d) and defluorination (Fig. 17e) within 120 minutes, representing near-complete mineralization. Long-term stability tests confirmed >95% degradation and defluorination over 10 cycles (Fig. 17f), while avoiding the formation of iron sludge commonly associated with traditional Fenton systems.

With the intention of elucidating the interaction mechanisms underlying PFOA degradation in the electro-Fenton reaction, Yu *et al.* conducted a systematic investigation on an Fe/N co-doped graphene electrode (Fe/N-GE@GF) (Fig. 18a).[91] A synergistic electrochemical process at the cathode was
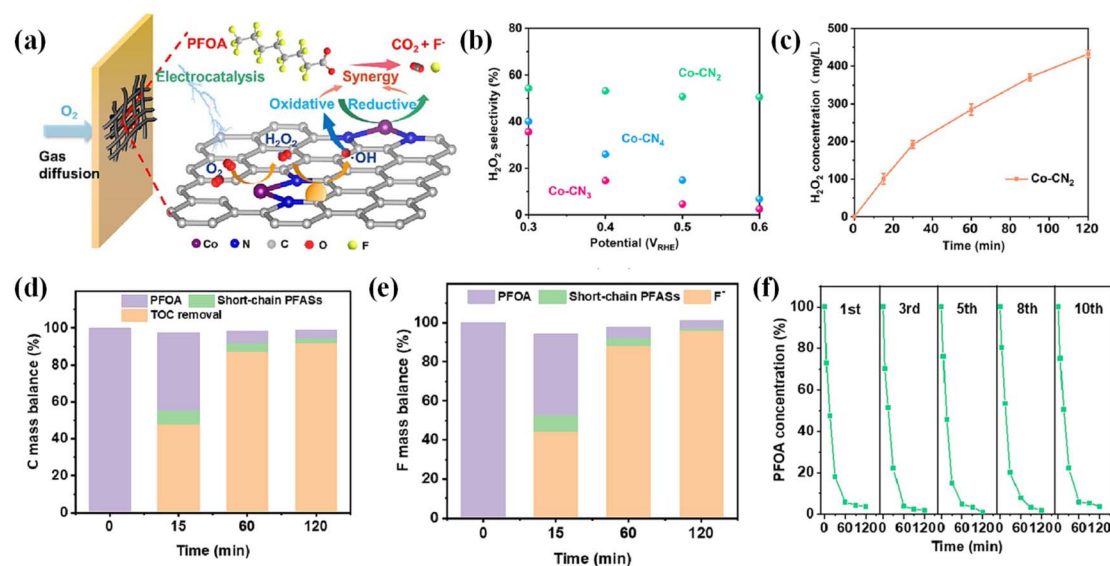
Fig. 17 (a) Schematic of PFOA degradation in the Co-CN$_2$-Fe$_2$O$_3$ cathode electro-Fenton process. (b) The calculated H$_2$O$_2$ selectivity as a function of the applied potentials. (c) Concentrations of H$_2$O$_2$ produced with Co-CN$_2$ as a function of electrolysis time. (d) C and (e) F mass balance during PFOA degradation over Co-CN$_2$-Fe$_2$O$_3$. (f) The recyclability of Co-CN$_2$-Fe$_2$O$_3$ for electro-Fenton PFOA degradation.[90]
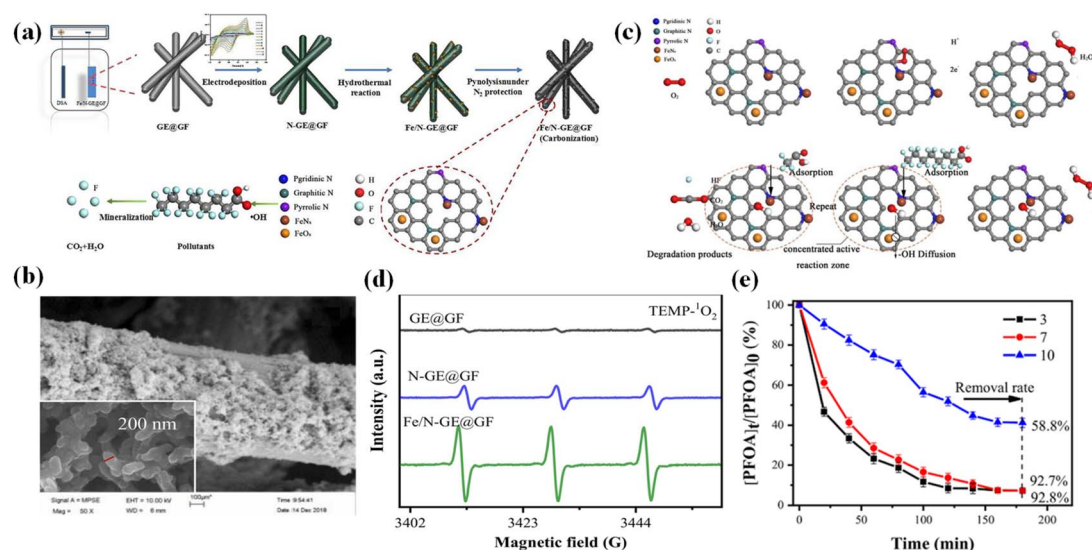
Fig. 18 (a) Schematic diagram of Fe/N-GE@GF preparation and degradation experiments. (b) SEM images of N-GE@GF. (c) Possible catalytic mechanism of Fe/N-GE@GF for PFOA degradation. (d) DMPO-$^1O_2$ by GE@GF, N-GE@GF and Fe/N-GE@GF cathodes in the electrocatalytic process. (e) PFOA adsorption performance of Fe/N-GE@GF at different pH values.[91]

proposed, and key factors influencing the efficiency of the electro-Fenton reaction were scientifically explored. The co-doping of Fe and N introduced significant lattice distortion and structural defects in the graphene framework, resulting in increased surface area and abundant microporosity (Fig. 18b). These features exposed more active sites for PFAS degradation. Moreover, N-containing precursors such as pyridine promoted uniform Fe dispersion and the formation of a robust three-dimensional porous structure. The presence of N also enabled PFAS molecules to interact with the electrode material, facilitating their enrichment near the reactive zones. Through precise spatial overlap of radical generation sites and PFAS accumulation regions (Fig. 18c), a "Focused Active Reaction Region" that significantly improved degradation efficiency was established. This system achieved 95% PFOA degradation, 90% total organic carbon (TOC) removal, and 80% defluorination within 3 hours. Notably, the Fe/N-GE@GF electrode was capable of generating ˙OH under neutral conditions by leveraging singlet oxygen ($^1O_2$) as a supplementary oxidant (Fig. 18d), thereby overcoming the classical Fenton system's dependence on pH environments. Under neutral conditions (pH = 7), the PFOA degradation efficiency of Fe/N-GE@GF was nearly identical to that observed under acidic conditions (pH = 3), reaching 92.7% compared to 92.8%. In contrast, a marked decrease in degradation efficiency was observed under alkaline conditions (pH = 10), though a considerable efficiency of 58.8% was still achieved (Fig. 18e).
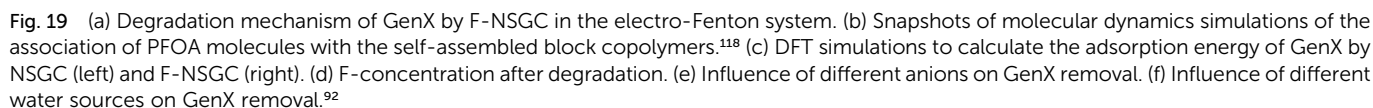
3.2.2 Iron-free cathodes. While iron-containing cathodic materials have attracted considerable attention, certain unique structural features of iron-free cathodes also exhibit interactions relevant to PFAS degradation. Wang *et al.* developed an iron-free biomass-derived nitrogen and sulfur self-doped porous carbon electrode (NSGC) for electro-Fenton degradation of hexafluoropropylene oxide dimer acid (GenX) (Fig. 19a), a widely used

substitute for the banned PFOA.[92] Previous studies have demonstrated that fluorine–fluorine (F···F) interactions between perfluorinated polymers and the perfluoroalkyl chains of PFOA play a critical role in enhancing adsorption from aqueous solutions (Fig. 19b).[118] The incorporated perfluoropolyether into the NSGC framework exhibited hydrophobic and fluorophilic characteristics, and significantly enhanced performance for GenX removal, that is consistent with the DFT calculation results, where the adsorption energy of Gen-X on F-NSGC was significantly enhanced from −35.93 kJ mol^{-1} to −46.91 kJ mol^{-1} in the presence of F–F interactions (Fig. 19c). In the electro-Fenton system, F-NSGC achieved an electro-adsorption efficiency of 59% for GenX within 60 minutes, followed by a degradation efficiency of 96% and a defluorination efficiency of 63% after 180 minutes (Fig. 19d). These results indicate both excellent degradation capacity and promising mineralization potential. The presence of competing anions exhibited negligible impact, with removal efficiencies exceeding 95% in all tested scenarios (Fig. 19e). When applied to real water samples—including lake water, secondary effluent from a municipal wastewater treatment plant, and tap water—the system consistently achieved over 90% GenX removal within 180 minutes (Fig. 19f). To further explore the application potential of this method, the reaction setup was adapted to continuous-flow reactors. Under a flow rate of 5 mL min^{-1} with a circulation time of 180 min, the GenX removal efficiency of up to 94% was achieved. However, excessively low flow rates reduced the contact between GenX and the catalytic material, thereby limiting the overall degradation efficiency.

With the aim of broadening the applicability of combined electro-oxidation and electro-Fenton systems for PFAS treatment, Luu *et al.* conducted a comprehensive evaluation of the Fenton-assisted electrochemical advanced oxidation process for the removal of 29 representative PFAS compounds, including both long- and short-chain species, as well as linear and

© 2026 The Author(s). Published by the Royal Society of Chemistry

Environ. Sci.: Adv., 2026, **5**, 9–42 | 23

Fig. 19 (a) Degradation mechanism of GenX by F–NSGC in the electro-Fenton system. (b) Snapshots of molecular dynamics simulations of the association of PFOA molecules with the self-assembled block copolymers.[118] (c) DFT simulations to calculate the adsorption energy of GenX by NSGC (left) and F–NSGC (right). (d) F-concentration after degradation. (e) Influence of different anions on GenX removal. (f) Influence of different water sources on GenX removal.[92]

branched isomers.[93] Ti/BDD and Ti/IrO$_2$ were used as anode materials for comparison, with Pt serving as the cathode. Fe$_3$O$_4$ nanoparticles were directly introduced into the reaction system as catalysts to enhance Fenton reactions. The researchers systematically optimized operational parameters such as pH, Fe$_3$O$_4$ concentration, current density, electrolysis duration, and electrolyte concentration. Under optimized conditions, removal efficiencies ranging from 86% to 100% were achieved within 120 minutes, with a low energy consumption of just 9.0 kWh m^3 (Fig. 20a and b). Following the attainment of high PFAS removal efficiencies, the study further investigated intermediate

products and degradation pathways. Using mass spectrometry and kinetic modeling, the plausible mineralization mechanisms were proposed (Fig. 20c). These mechanistic insights provide valuable references for treating other recalcitrant organic pollutants using electro-Fenton-based approaches.

Electro-Fenton reactions have demonstrated the capability for rapid PFAS degradation, accompanied by significant improvements in defluorination efficiency. Notably, by expanding the sources of oxygen, the electro-Fenton process has overcome the pH limitations inherent to traditional chemical Fenton systems, enabling the *in situ* generation of ˙OH under

Fig. 20 (a) PFAS removal efficiency *via* the Fenton-assisted electrochemical oxidation process. (b) Energy consumption *via* the Fenton-assisted electrochemical oxidation process. (c) Intermediate compounds and degradation pathway of PFBS.[93]
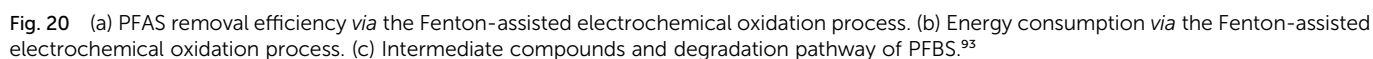
neutral conditions without the need for external H_2O_2 addition, while also substantially reducing the formation of iron sludge. However, several challenges remain. One of the primary limitations is the high energy consumption associated with the electro-Fenton process, which has increasingly drawn attention focused on techno-economic assessments. Reducing energy demand thus represents a critical direction for future development. Additionally, improvements in the durability and stability of electrode materials are necessary to achieve more favorable life-cycle performance. At present, most research remains at a preliminary or laboratory scale, and there is a pressing need for comprehensive evaluation data on the treatment of large-scale contaminated water systems.

3.3 Photo-Fenton reaction systems

Compared to electro-Fenton systems, which rely on externally applied electric power to drive electron transfer processes, photo-Fenton reactions are generally considered to be a greener and more environmentally friendly class of AOPs (Fig. 21).[119,120] In a photo-Fenton system, UV or visible light irradiation facilitates the photoreduction of ferric complexes to Fe^{2+}, thereby accelerating the decomposition of H_2O_2. Specifically, under mildly acidic conditions (pH 2.8–3.5), Fe^{3+} forms light-responsive ferric hydroxo complexes, such as $[Fe(OH)]^{2+}$,[68,121] which can undergo ligand-to-metal charge transfer (LMCT) excitation, regenerating Fe^{2+} and promoting further $\cdot OH$ production.[122] Recent studies have also shown that Fe^{3+} can form complexes with PFAS anions, and these complexes may exhibit enhanced photo-response under irradiation, facilitating PFAS degradation.

Although solar light is more widely available and cost-effective, the efficient control and utilization of photonic

energy remain a key research challenge in photo-Fenton systems.[123] These systems are typically classified into homogeneous and heterogeneous processes, depending on the physical state of the catalyst. In homogeneous photo-Fenton systems, both the catalyst and reactants are dissolved in aqueous media, providing high dispersibility and intimate contact with contaminants. However, the generally poor light absorption capacity of homogeneous species limits their degradation efficiency, making this a focus for further optimization. In contrast, heterogeneous photo-Fenton systems exhibit greater capability for absorbing and converting light into chemical energy. Photoinduced holes generated on solid catalyst surfaces can effectively participate in PFAS degradation. Nonetheless, rational design of the catalyst surface and optimization of PFAS mass transfer to reactive sites remain essential considerations for performance improvement.

3.3.1 Homogeneous photo-Fenton systems. Homogeneous photo-Fenton reactions were developed earlier than their heterogeneous counterparts due to no complex catalyst design or synthesis steps required.[124] The fundamental mechanism of PFAS degradation in homogeneous photo-Fenton systems has been relatively well elucidated. However, limited solubility and recovery challenges of homogeneous catalysts have constrained the application for PFAS degradation.

To verify the feasibility of PFAS degradation *via* the photo-Fenton process, Tang *et al.* developed a homogeneous ultraviolet-assisted photo-Fenton system with ferric and ferrous sulfate dissolved in PFOA solution (Fig. 22a).[94] The influence of reagent stoichiometry (*i.e.*, concentrations of Fe^{2+} and H_2O_2) and solution pH on PFOA degradation efficiency was systematically investigated. An optimal Fe^{2+} concentration of 2.0 mM

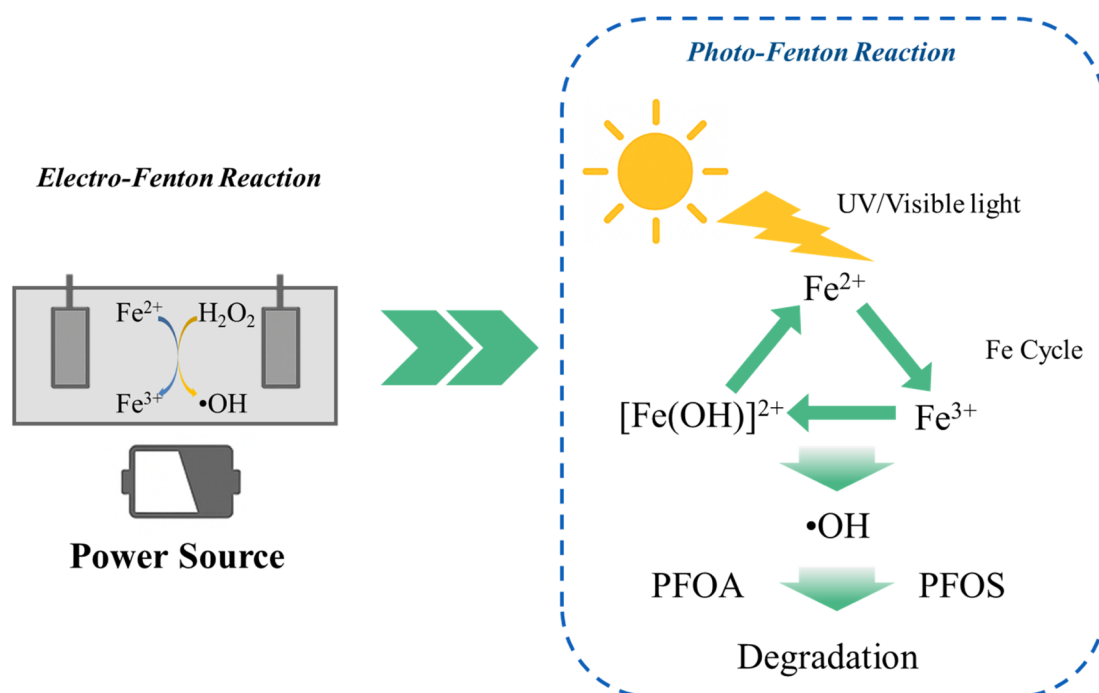**Fig. 21** Comparison between electro-Fenton and photo-Fenton systems for the degradation of PFASs.

© 2026 The Author(s). Published by the Royal Society of Chemistry
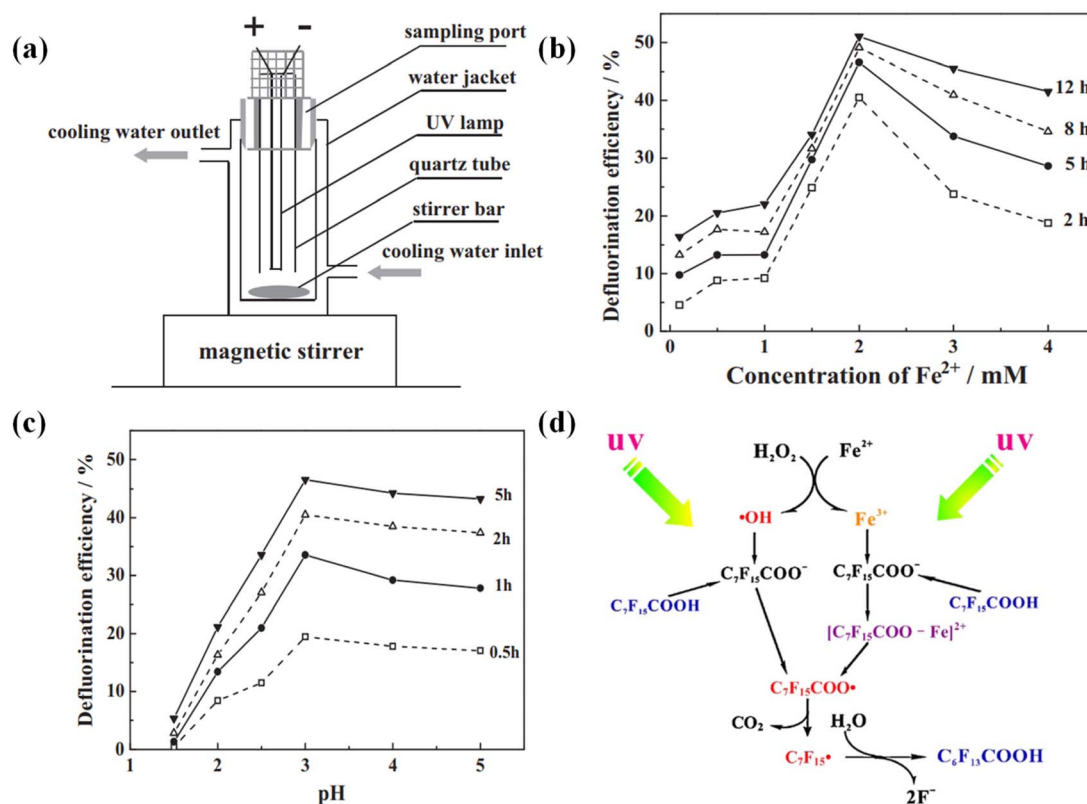
Environ. Sci.: Adv., 2026, **5**, 9–42 | **25**

Fig. 22 (a) The diagram of the experimental set-up for homogeneous photo-Fenton degradation of PFOA. (b) Effects of initial Fe^{2+} concentration on the defluorination efficiency of PFOA. (c) Effects of H_2O_2 concentration on the defluorination efficiency of PFOA. (d) A two-stage mechanism for the degradation of PFOA in the homogeneous photo-Fenton process.[94]

was identified: at this level, more $^{\bullet}OH$ radicals were generated to enhance both PFOA degradation and defluorination (Fig. 22b). However, excessive Fe^{2+} could also act as a scavenger for $^{\bullet}OH$, thereby reducing the availability of reactive species for PFAS oxidation. Solution pH was found to play a critical role (Fig. 22c). At pH < 2.0, H_2O_2 is readily protonated to form $H_3O_2^+$, decreasing its reactivity with Fe^{2+}. At pH > 4.0, Fe^{3+} tends to hydrolyze rapidly, forming $Fe(OH)_3$ precipitates, which hinder both light penetration and complexation with PFOA. Accordingly, the optimal pH range for homogeneous photo-Fenton reactions was determined to be between 2.8 and 3.5.

In addition to $^{\bullet}OH$, the interaction between Fe^{3+} and PFOA contributed to the enhancement of the degradation process. A two-stage degradation mechanism was proposed (Fig. 22d). In the initial stage, $^{\bullet}OH$ is present in sufficient concentrations to directly activate PFOA anions, forming $^{\bullet}C_7F_{15}$ radicals. These radicals further react with $^{\bullet}OH$ to generate $C_7F_{15}OH$, which undergoes hydrolysis and HF elimination to yield short-chain PFAS intermediates, CO_2, and HF. In the second stage, once $^{\bullet}OH$ is depleted, Fe^{3+} forms a $[C_7F_{15}COO–Fe]^{2+}$ complex with PFOA, which, under UV irradiation, is photo-reduced to Fe^{2+} and a carboxyl radical ($C_7F_{15}COO^{\bullet}$), initiating another degradation cycle with the limited $^{\bullet}OH$ available.

In order to further broaden the spectral utilization of the photo-Fenton process, Alvarez et al. extended the conventional UV-based photo-Fenton system by introducing visible light as an alternative irradiation source.[95] The potential of utilizing visible light to effectively drive the photo-Fenton degradation of PFOA was demonstrated. Visible light, as one of the most green and renewable energy sources, offers significant advantages for photo-Fenton degradation of PFOA. It greatly reduces the energy consumption of the reaction, enhances operational safety, and lowers equipment requirements. Therefore, visible light is considered an ideal energy input for such advanced oxidation processes. Electron paramagnetic resonance (EPR) spectroscopy confirmed that $^{\bullet}OH$ was the primary reactive species (Fig. 23a and b). However, the process required prolonged treatment—28 days—to achieve 98% PFOA degradation (Fig. 23c), with only 13% defluorination, highlighting limitations in efficiency, particularly for the degradation of short-chain PFASs. A plausible mechanism for PFAS degradation via the photo-Fenton process was also proposed, which is generally consistent with those suggested in previous studies. In this mechanism, $^{\bullet}OH$ not only directly attacks PFOA but may also target the $[C_7F_{15}COO–Fe]^{2+}$ complex. Fe^{3+} is believed to further reduce the activation energy barrier for $^{\bullet}OH$-mediated PFOA degradation. Additionally, a more detailed pathway for the formation of intermediates was presented, indicating broader recognition of this mechanism (Fig. 23d).

To further enhance the degradation efficiency of the homogeneous photo-Fenton reaction and to gain a more comprehensive understanding of its underlying mechanism, Zhang
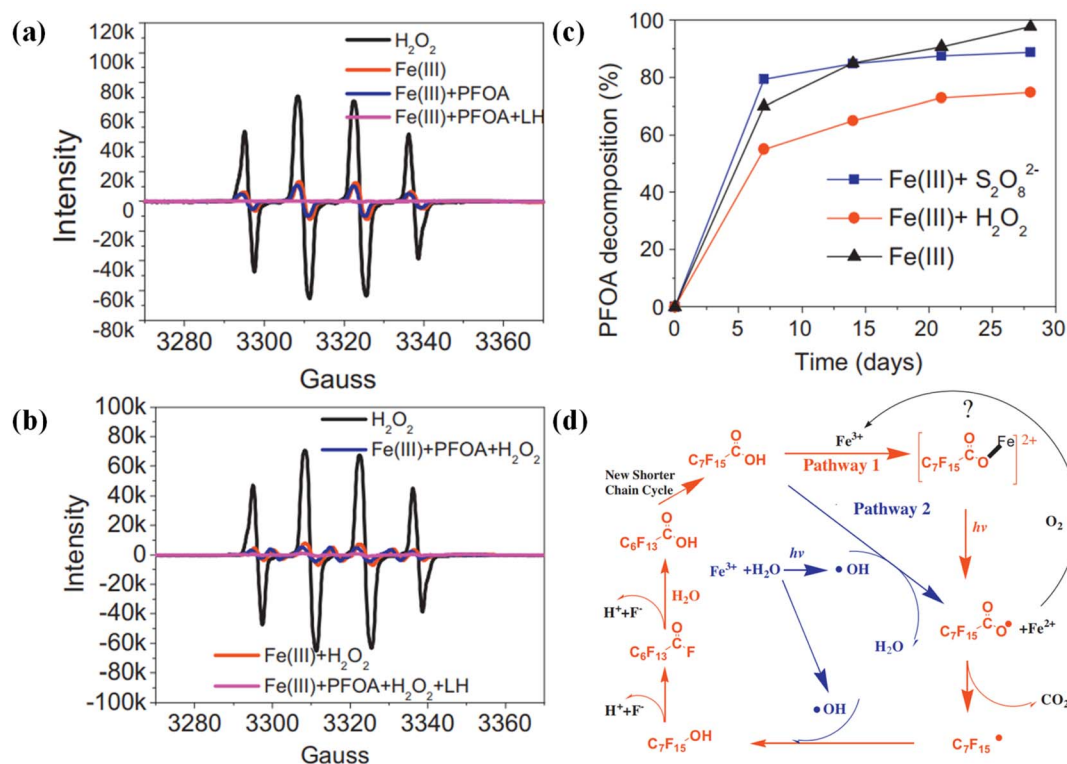
Fig. 23 (a) EPR spectra of radicals generated in different experimental groups. (b) EPR spectra of radicals generated in the Fe(III)−H_2O_2 (2 mM) system; EPR samples were taken after 10 min UV irradiation. (c) Comparison of PFOA degradation by different reaction systems. (d) Proposed PFOA degradation pathway in the presence of Fe(III) and sunlight.[95]

et al. developed a hybrid system combining Fe^0/granular activated carbon (Fe^0/GAC) microelectrolysis with a vacuum UV-Fenton (VUV-Fenton) process for PFOA mineralization.[96] In this system, Fe^0/GAC was first mixed with PFOA to generate numerous microscale galvanic cells that continuously supplied electrons and Fe^{2+} ions, facilitating the initial breakdown of the PFOA structure through enhanced electron transfer (Fig. 24a).

Following a pre-activation step, the photo-Fenton reaction was conducted under UV irradiation at 254 nm (Fig. 24b), resulting in a defluorination efficiency of 47%, which represents a notable improvement compared to the 39% achieved using the VUV-Fenton system alone (Fig. 24c). High-performance liquid chromatography tandem mass spectrometry (HPLC/MS/MS) was employed to identify and quantify degradation

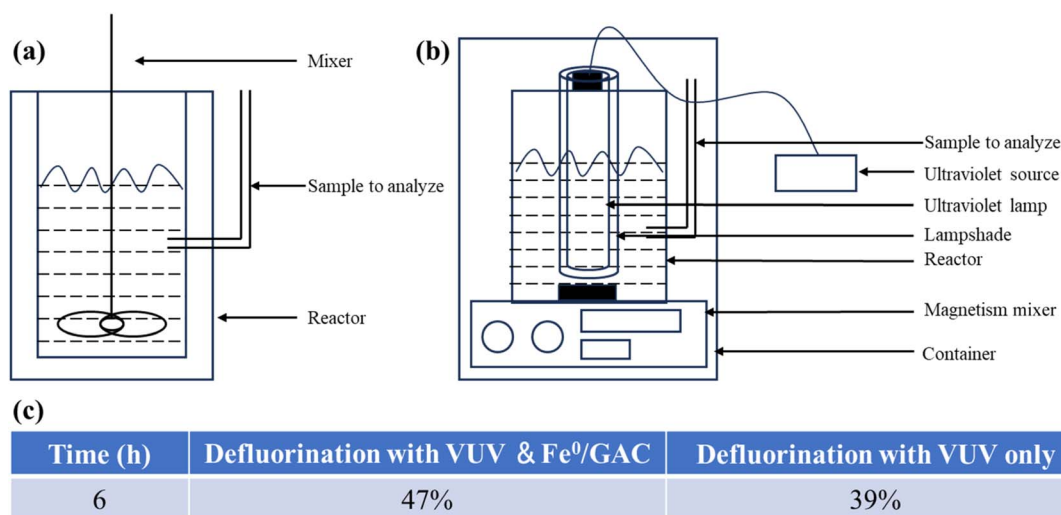| Time (h)	Defluorination with VUV & Fe^0/GAC	Defluorination with VUV only
6	47%	39%

Fig. 24 (a) Schematic representation of reactor iron−carbon micro-electrolysis and (b) VUV-Fenton. (c) Photochemical defluorination ratio under VUV and Fe^0/GAC micro-electrolysis and VUV-Fenton systems.

intermediates. The detected short-chain perfluorocarboxylic acids (PFCAs)—including PFHpA (C7), PFHeA (C6), PFPeA (C5), PFBA (C4), PFPrA (C3), and TFA (C2)—further confirmed the proposed degradation mechanism of PFOA under photo-Fenton conditions.

3.3.2 Heterogeneous photo-Fenton systems. Compared to homogeneous photo-Fenton reactions, heterogeneous photo-Fenton systems typically utilize iron-containing catalysts, which can reduce the need for additional anions and facilitate catalyst recovery through the magnetic properties of solid-phase iron. Based on this concept, Urtiaga *et al.* employed a TiO_2/ reduced graphene oxide composite catalyst (95% TiO_2/5% rGO) for the photo-Fenton degradation of PFOA.[97] After 12 hours of UV-visible irradiation using a mercury lamp, the PFOA degradation efficiency of TiO_2-rGO reached $93 \pm 7\%$, representing a substantial improvement compared with TiO_2 photocatalysis ($24 \pm 11\%$ removal) and direct photolysis ($58 \pm 9\%$) (Fig. 25a). It was reasonably hypothesized that rGO effectively captured photogenerated electrons from TiO_2, thereby suppressing electron–hole recombination (Fig. 25e). This process promoted PFOA degradation through direct oxidation by photogenerated holes or *via* reactive radical pathways. The progressive decomposition mechanism was further supported by the identification of short-chain perfluorocarboxylic acids (Fig. 25b) and the release of fluoride ions (Fig. 25c), which closely matched the reduction in total organic carbon (Fig. 25d), in line with a stepwise degradation pathway mediated by photogenerated

hydroxyl radicals. These findings strongly verified the critical role of ˙OH radicals and the stepwise degradation mechanism in PFOA removal by TiO_2-rGO. Moreover, kinetic studies revealed a clear correlation between degradation efficiency and molecular structure, as the apparent first-order rate constants for UV-visible degradation of PFOA and its intermediate perfluorocarboxylic acids increased with decreasing carbon chain length (Fig. 25b). In summary, the development of a heterogeneous photo-Fenton system based on TiO_2-rGO provides a feasible strategy for PFAS degradation and offers detailed mechanistic insights, thereby laying a solid scientific foundation for future research.

In order to achieve a more uniform distribution of iron on the catalyst surface and to elucidate the mechanism of heterogeneous photo-Fenton degradation of PFASs, Wang *et al.* synthesized a cellulose-based membrane ($Co_3O_4@Fe_3O_4$) by coating Co_3O_4 nanoparticles onto rod-like MOF-derived Fe_3O_4 and incorporating the composite into a cellulose solution (Fig. 26a). This membrane was then applied in a visible-light-driven photo-Fenton system,[98] where efficient energy conversion and a rich reactive radical environment enabled effective PFOA degradation. The degradation mechanism relied on the synergistic interplay among photogenerated electrons, holes (h^+), and various reactive species rather than a single dominant species. The photogenerated h^+ directly attacked the carboxylic group (—COOH) of PFOA, initiating decarboxylation and forming $C_7F_{15}^{\bullet}$ radicals. The electrons (e^-) reduced dissolved
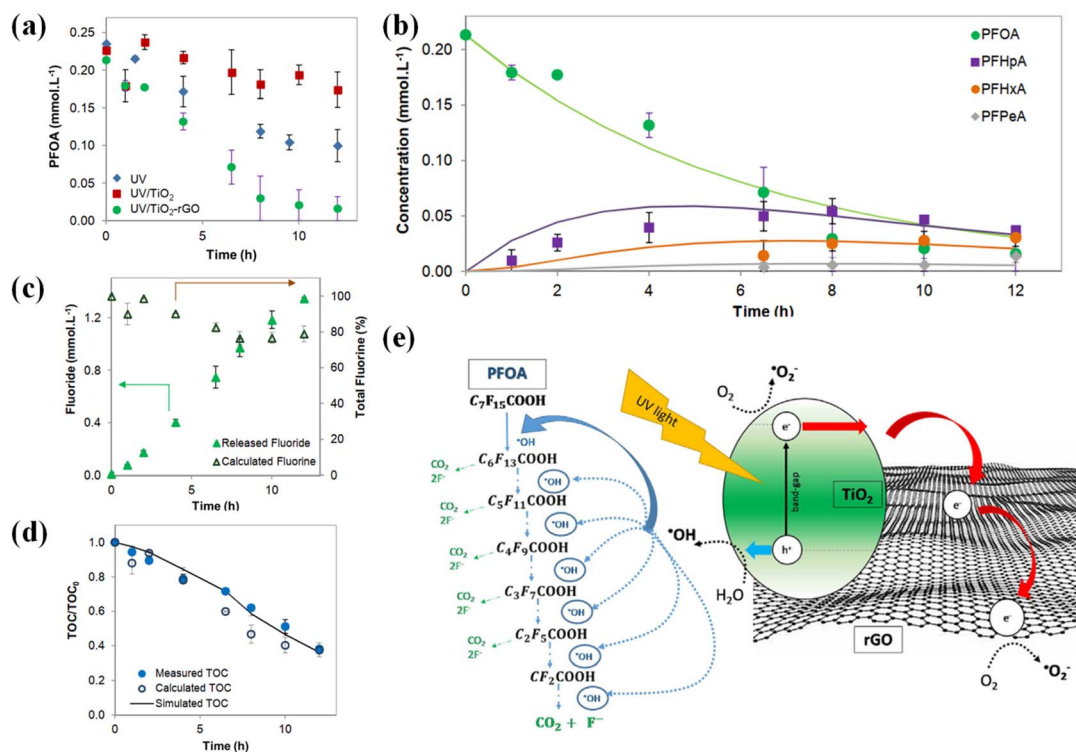
Fig. 25 (a) Evolution of PFOA concentration with irradiation time by photolysis and photocatalysis using TiO_2 and TiO_2-rGO. (b) Evolution of PFOA, PFHpA, PFHxA and PFPeA, and their simulated concentrations using the pseudo-first order estimated kinetic parameters. (c) Fluoride in solution and calculated total fluorine. (d) Measured TOC/TOC^0, calculated TOC/TOC^0 from the analyzed PFASs, and simulated TOC/TOC^0 using the simulated PFAS concentrations. (e) Photocatalytic pathways of PFOA decomposition using the TiO_2-rGO catalyst.[97]

Fig. 26 (a) Schematic illustration of the steps to prepare $Co_3O_4@Fe_3O_4$/cellulose blend membranes. (b) Type-II heterojunction reaction mechanism. (c) Reusability of the blend membrane. (d) Proposed degradation pathway of PFOA in the H_2O_2/membrane/visible light system.[98]

oxygen to $O_2^{\cdot-}$, which contributed to further degradation, and also regenerated Fe^{2+} from Fe^{3+}, maintaining $\c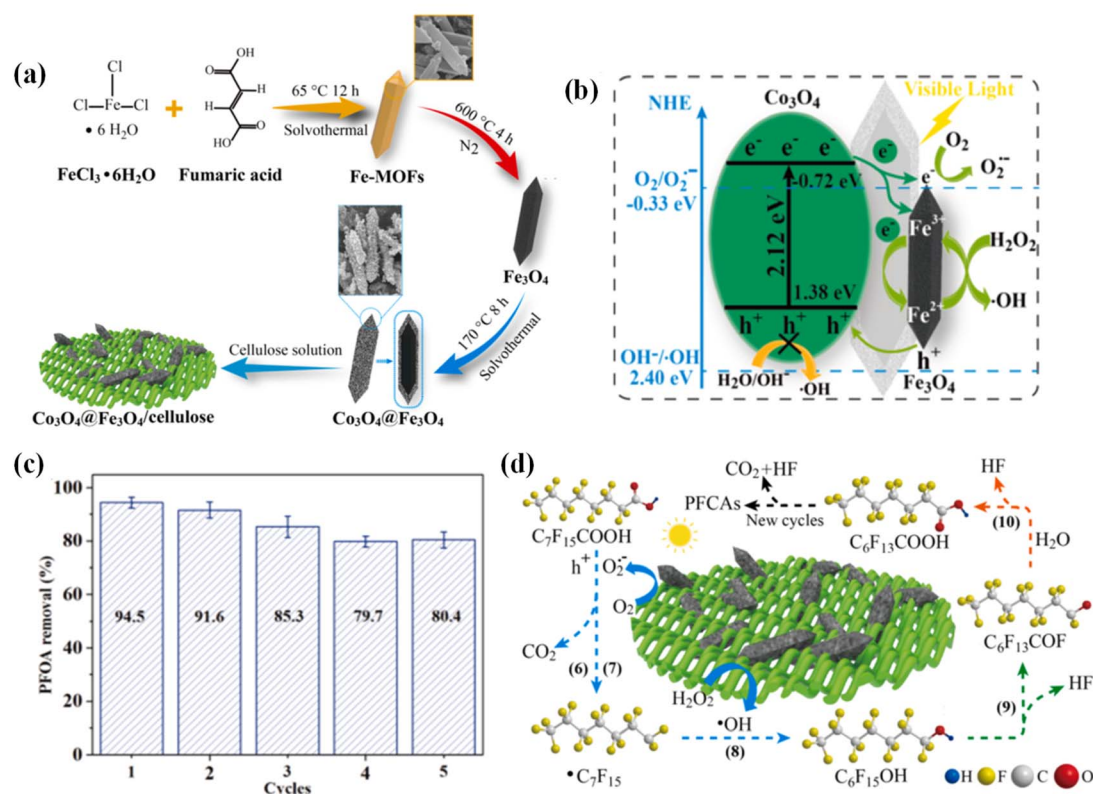dot OH$ production (Fig. 26b). The $Co_3O_4@Fe_3O_4$ membrane demonstrated outstanding performance, achieving 95% PFOA degradation, retaining 80% efficiency after five cycles (Fig. 26c), and exhibiting minimal metal leaching (Fe: 0.05 ppm; Co: 0.49 ppm). These results were attributed to the material's architecture: regenerated cellulose formed a 3D porous network under alkaline/urea/thiourea conditions, which helped disperse the $Co_3O_4@Fe_3O_4$ nanoparticles and prevent aggregation (Fig. 26d). This study provides valuable experimental and theoretical insights into the rational design of heterogeneous photo-Fenton catalysts.

To elucidate the synergistic mechanism between PFAS adsorption and photoactivity, Zhang et al. developed ZIF-67@C_3N_4 and MIL-100(Fe)@C_3N_4 composites with high specific surface areas and adsorption capacity for photo-Fenton degradation of PFOA (Fig. 27a and b).[99] Experimental results revealed that ZIF-67@C_3N_4 and MIL-100(Fe)@C_3N_4 achieved PFOA removal efficiencies of 79.2% and 60.5% (Fig. 27c and d), respectively—substantially higher than unmodified C_3N_4. Quenching experiments indicated that photogenerated holes (h^+) played the primary role in photo-Fenton PFOA degradation, mainly by directly attacking PFOA molecules adsorbed on the catalyst surface and oxidizing water to produce $\cdot OH$ (Fig. 27e). Beyond the photon-induced pathways, PFOA adsorption and

charge separation mechanisms also contributed to the high degradation efficiency, such as the catalyst's ability to accumulate PFOA near photoactive C_3N_4 sites, the enhanced visible-light absorption and charge separation induced by heterojunctions.

Integrating the heterogeneous photo-Fenton reaction and material structure design for enhancing the radical reactivity, Chen et al. developed Fe(III)-saturated porous montmorillonite (Fe-MMT) as a heterogeneous catalyst to enhance the photo-Fenton reaction.[100] The pore structure microenvironment facilitates effective collisions between $\cdot OH$ and PFOA, thereby establishing an alternative strategy for PFOA degradation. In a system containing 1 g L^{-1} Fe-MMT and 24 μM PFOA, approximately 90% of the initial PFOA was degraded within 48 hours. The enhanced degradation was attributed to the generation of reactive oxygen species and the LMCT mechanism involving Fe species in the interlayer of MMT. Fe^{3+} coordinated with the carboxylate group ($-COO^-$) of PFOA to form a PFOA–Fe^{2+} complex (Fig. 28a). Upon UV irradiation, electrons were transferred from the PFOA ligand to the Fe^{3+} center, producing $\cdot C_7F_{15}COO$ radicals and Fe^{2+}. This LMCT process significantly lowered the activation free energy for PFOA oxidation from 163 to 59.3 kJ mol^{-1} (Fig. 28b). Further experiments demonstrated that the UV/Fe-MMT system maintained high PFOA removal efficiency even in the presence of natural organic matter and inorganic ions, indicating strong anti-interference capability
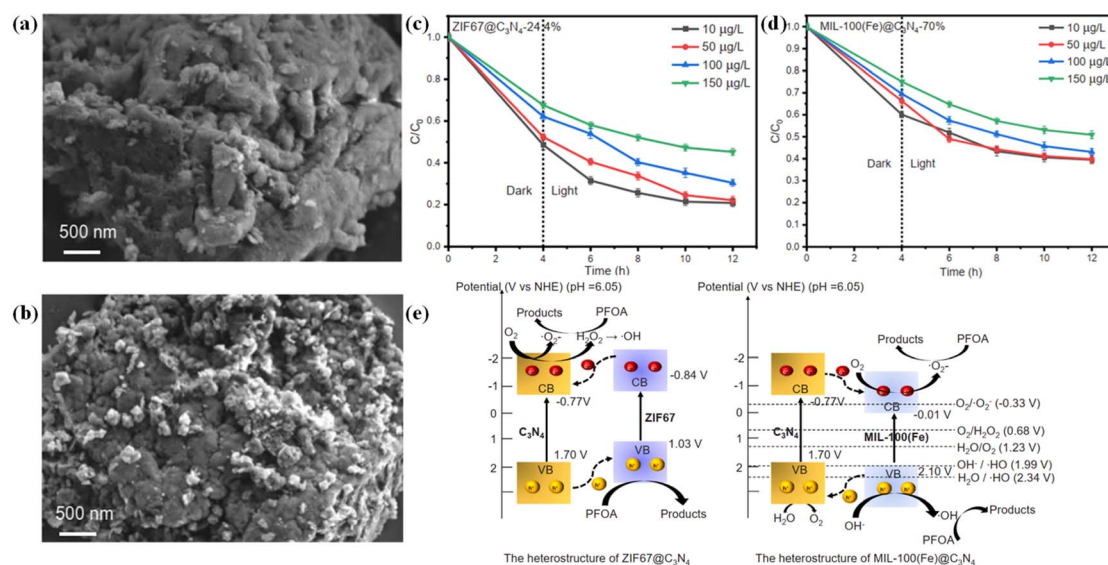
Fig. 27 SEM images of C_3N_4 (a) and MIL-100(Fe)@ C_3N_4 (b). Photodegradation of PFOA with the presence of ZIF67@C_3N_4-24.4% (c) and MIL-100(Fe)@C_3N_4-24.4% (d) with different initial concentrations of PFOA. (e) The heterostructure of ZIF67@C_3N_4 and MIL-100(Fe)@C_3N_4.[99]
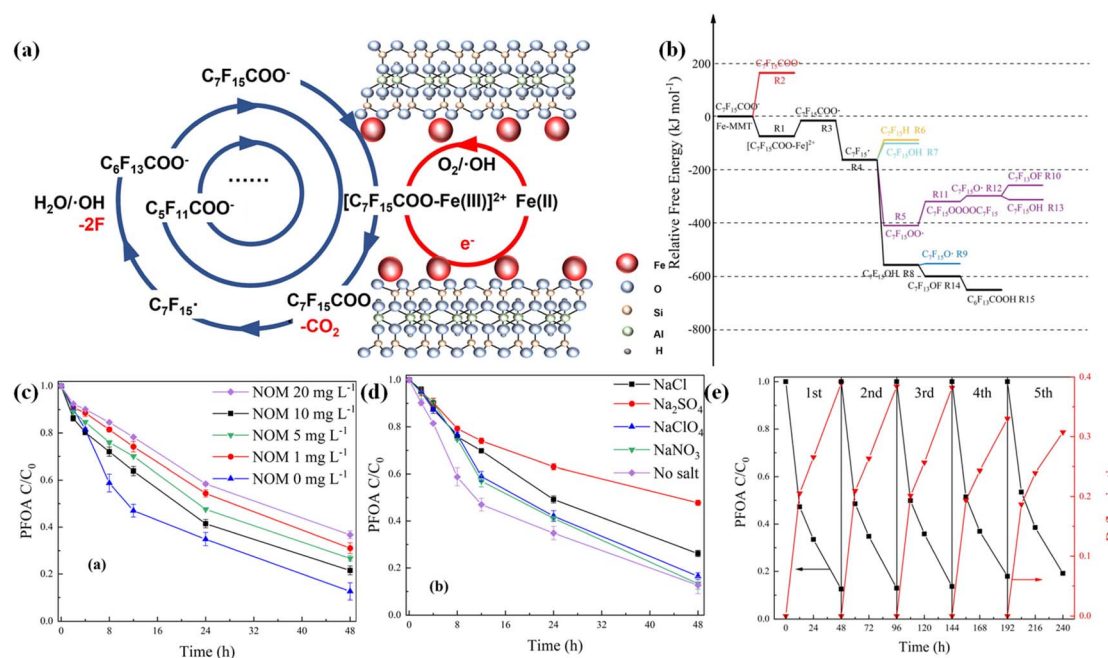
Fig. 28 (a) Proposed reaction mechanism for the photo-decomposition of the UV/Fe-MMT Fenton system. (b) Scheme of the potential energy surface for the degradation of PFOA in the presence of Fe-MMT. Effect of NOM (c) and inorganic ions (d) on PFOA degradation in the UV/Fe-MMT Fenton system. (e) PFOA degradation (black) and defluorination (red) in consecutive batch runs of the UV/Fe-MMT Fenton system.[100]

(Fig. 28c and d) and potential for practical applications in diverse wastewater treatment scenarios. Moreover, the Fe-MMT catalyst could be regenerated and reused, offering an economic advantage for industrial-scale PFOA remediation (Fig. 28e).

Besides experimental validation of scientific hypotheses, theoretical modeling also plays a crucial role in guiding experimental design. Zúniga-Benítez *et al.* systematically optimized the key parameters (ferrous ion concentration and hydrogen

peroxide concentration) for the ultraviolet photo-Fenton (UV/photo-Fenton) degradation of PFOA using response surface methodology (Fig. 29a and b).[101] Under optimal conditions (Fe^{2+} = 0.1675 g L^{-1}, H_2O_2 = 14.0 g L^{-1}, pH 3.0), a 99% removal efficiency was achieved within 60 minutes (Fig. 29c). Interestingly, the presence of natural water matrices (*e.g.*, TOC = 2.895 mg L^{-1}, nitrate) enhanced degradation efficiency. In untreated surface water, the degradation rate was

30 | *Environ. Sci.: Adv.*, 2026, **5**, 9–42

© 2026 The Author(s). Published by the Royal Society of Chemistry
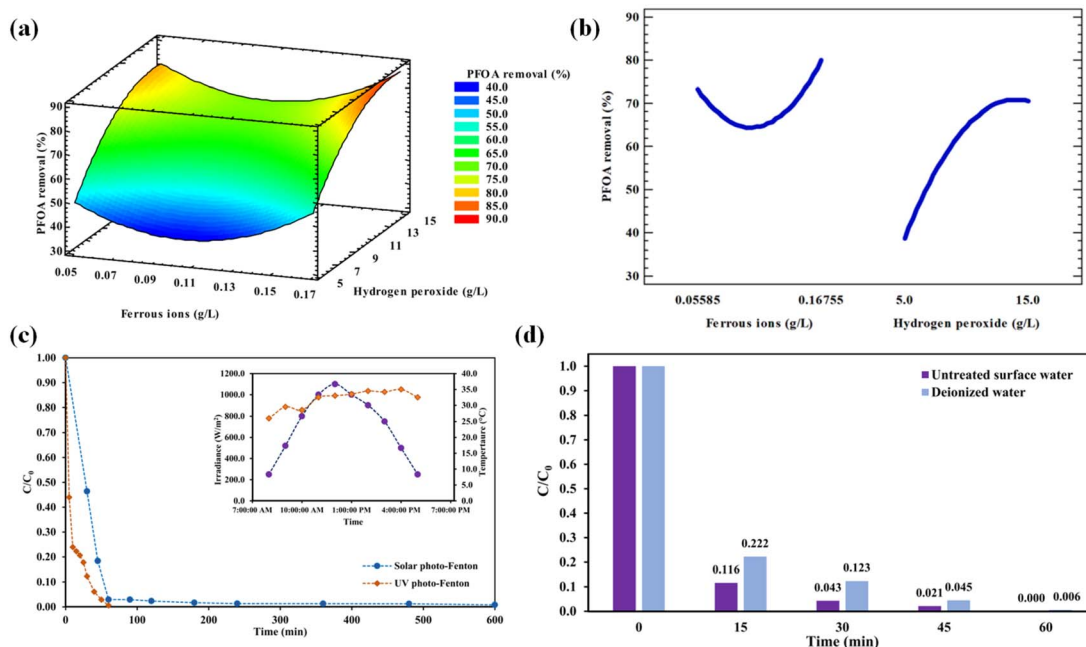
Fig. 29 (a) Response surface for PFOA removal using the photo-Fenton system. (b) Main effects plot for PFOA removal using the photo-Fenton system. (c) PFOA removal under optimized conditions using photo-Fenton and direct solar radiation. (d) Effect of the water matrix in the PFOA removal using the photo-Fenton system.[101]
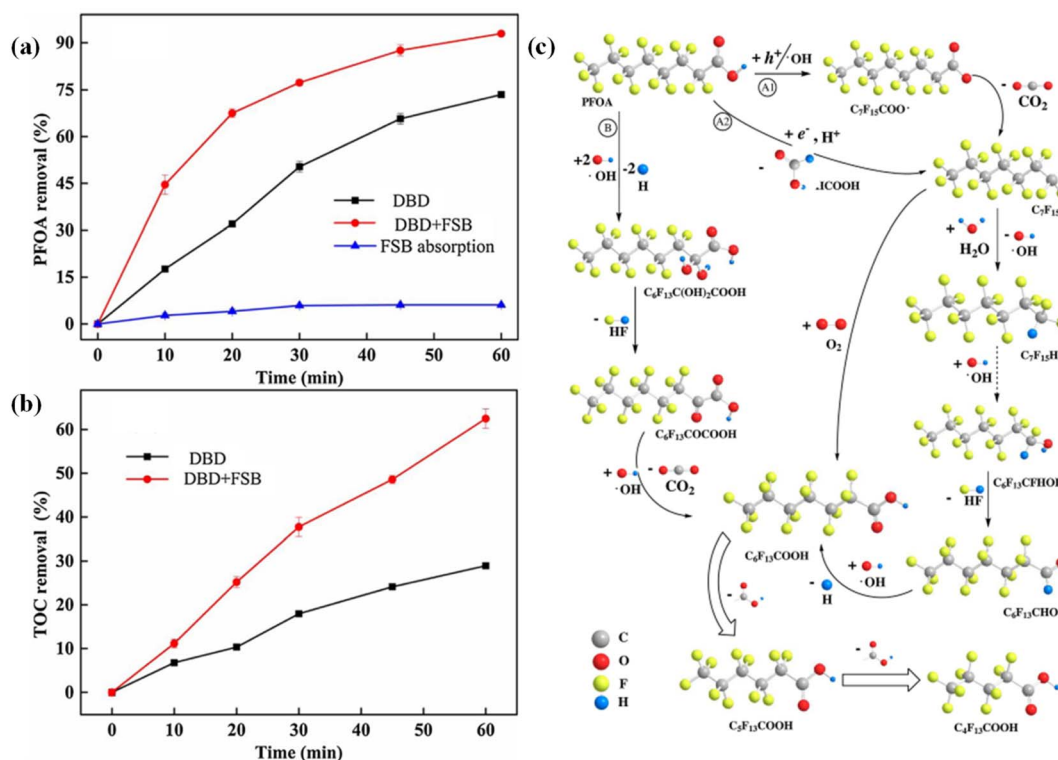
Fig. 30 (a) PFOA removals in different treatment processes. (b) TOC removals in different treatment processes. (c) Proposed mineralization mechanism of PFOA in the DBD-FSB system.[102]

approximately 30% faster than in deionized water. When UV irradiation was replaced with natural sunlight ($\lambda > 290$ nm), the system still achieved a 95% removal rate within 60 minutes under optimized conditions (Fig. 29d), suggesting that solar photo-Fenton processes offer a low-energy alternative particularly suited for sun-rich regions.

Homogeneous photo-Fenton reactions offer important mechanistic insights into the degradation pathways of PFASs, while heterogeneous photo-Fenton systems further reveal the structure–activity relationships between the material architecture and degradation performance. One of the most significant advantages of photo-Fenton processes is their use of renewable light energy, aligning closely with the principles of green and sustainable chemistry. However, compared to electro-Fenton systems that enable *in situ* H_2O_2 generation, the requirement for external H_2O_2 addition in photo-Fenton reactions remains a notable limitation. Furthermore, current research is predominantly focused on UV light-driven systems, which, although effective, often entail higher energy consumption. Although visible light has also been demonstrated to activate photo-Fenton processes for PFAS degradation, the technological maturity of such systems still requires further advancement. Additionally, the scope of photo-Fenton treatment must be broadened to a wider range of PFAS species, particularly those with more complex molecular structures and diverse chemical bond types, which demand more robust and efficient degradation strategies.

3.4 Solar photo-electro-Fenton (SPEF) systems

SPEF systems represent a promising and emerging advancement in the development of Fenton-based processes. By integrating the benefits of photo-assisted and electrochemical Fenton mechanisms, SPEF systems build upon traditional chemical Fenton reactions to offer a greener and more energy-efficient approach for pollutant degradation. In particular, the $2e^-$-ORR generates *in situ* H_2O_2, reducing the need for external Fenton reagents. Simultaneously, photoinduced electron–hole transfer further enhances oxidative efficiency while minimizing energy input.[125] One of the major challenges in SPEF technology lies in the system design,[126] which must accommodate the simultaneous requirements of both photo-Fenton and electro-Fenton processes, posing considerable demands on the catalyst architecture and operational compatibility.

As an initial attempt to apply photo-electro-Fenton reactions for PFAS degradation, Yu *et al.* developed a magnetic $Fe_3O_4@$-SiO_2-BiOBr (FSB) composite, which was integrated into a dielectric barrier discharge (DBD) reactor and employed as a heterogeneous Fenton-like photocatalyst for PFOA degradation.[102] The system effectively established a photo-electro-Fenton framework. Compared to DBD alone, the DBD-FSB
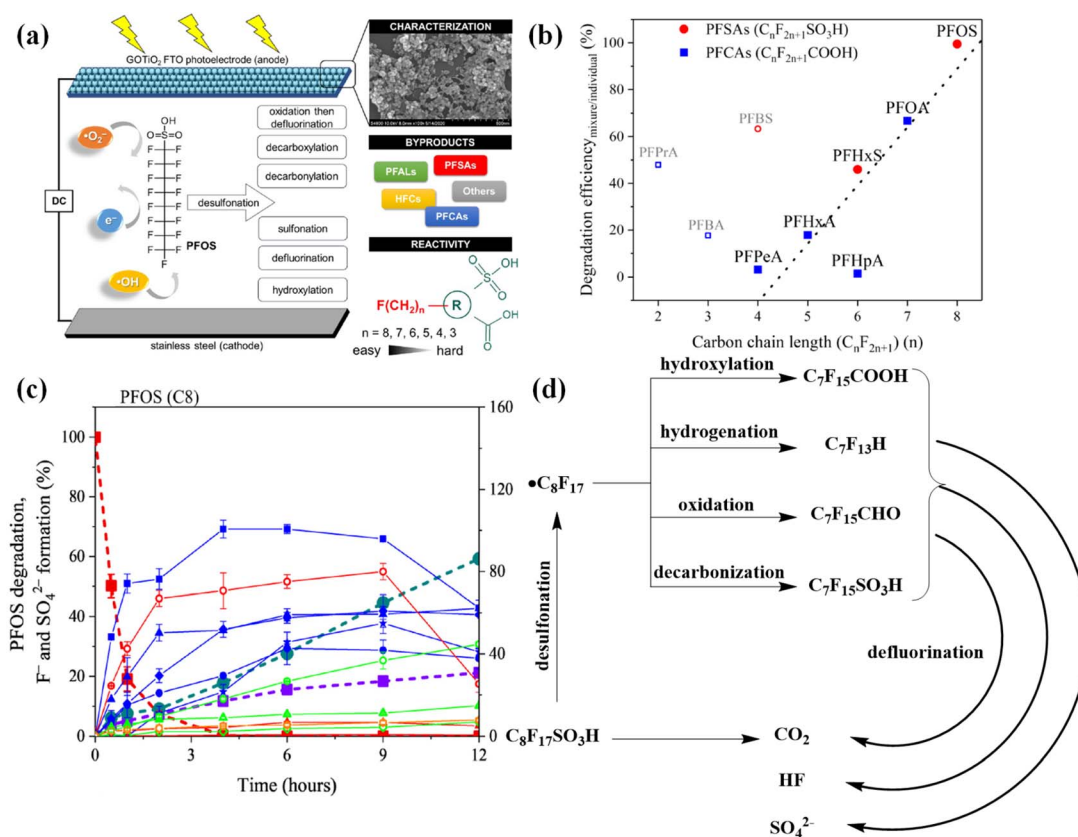

Fig. 31 (a) Schematic of PFOS degradation in the photoelectrochemical system. (b) The relationship between the carbon chain length and degradation efficiency ratio ($\eta_{mixture}/\eta_{individual}$) of PFASs. (c) Formation of the transformation byproducts, F^- and SO_4^{2-} from PFOS degradation in PEC systems.[103] (d) Proposed degradation pathway of PFOS in the PEC system.

system enhanced PFOA removal from 74% to 93% and TOC removal from 29% to 63% within 60 minutes (Fig. 30a and b). The energy efficiency also increased significantly from 46.4 mg kW^{-1} h^{-1} to 72.5 mg kW^{-1} h^{-1}. This performance was attributed to multiple reactive species pathways: (i) generation of ˙OH, H$_2$O$_2$, and O$_3$ by DBD plasma; and (ii) light-induced Fenton-like reactions on FSB. Multiple PFOA degradation pathways were proposed (Fig. 30c), including: (1) hole-driven decarboxylation and radical formation on FSB; (2) direct oxidation in the plasma discharge; and (3) hydroxyl radical attack at the α-CF$_2$ site, triggering defluorination. The synergistic design improved both degradation efficiency and mechanistic understanding.

Subsequently, to further refine the photo-electro-Fenton system and expand the variety of reactive radical species, Lin et al. successfully fabricated a graphene oxide-titanium dioxide (GO-TiO$_2$) photoelectrode.[103] The efficient energy input of a photoelectrochemical (PEC) system and the synergistic effects of multiple reactive radicals significantly enhanced the Fenton reaction efficiency and PFOS remediation (Fig. 31a). The process involved electron transfer, hydroxyl radical generation, and superoxide anion radicals. The degradation pathway was investigated through the identification of 25 intermediate products, including perfluoroalkyl sulfonates (PFSAs) (Fig. 31b and c), perfluoroaldehydes (PFALs), and hydrofluorocarbons (HFCs). Two primary mineralization routes were proposed (Fig. 31d): one via stepwise conversion to shorter-chain PFSAs, and another involving initial transformation to PFOA-like structures followed by PFOA degradation. PFALs and HFCs were confirmed as oxidation byproducts of perfluoroalkyl

radicals (Fig. 31d). The study also showed that shorter-chain PFASs displayed lower degradation rates, indicating stronger resistance and competitive inhibition in PFAS mixtures.

The photo-electro-Fenton system was then further advanced into the SPEF system by utilizing a more sustainable and readily available light source—sunlight. Following the design principles of SPEF, Wang et al. introduced a dual-function MOF/carbon nanofiber (MOF/CNF) composite membrane (Fig. 32a) for efficient solar photo-electro-Fenton degradation of PFOA.[104] The bifunctional cathode was fabricated by solvothermal growth of Fe/Co bimetallic MOFs onto electrospinning PAN-derived CNFs, exhibiting both photo- and electrocatalytic activity. EPR analysis confirmed enhanced ˙OH generation under solar irradiation. The system achieved 99% PFOA removal within 120 minutes (Fig. 32b). XPS analysis revealed valence changes of Fe and Co, and a corresponding mineralization mechanism was proposed (Fig. 32c). In 2022, the same group advanced this design by integrating a glucose fuel cell (GFC) with the SPEF system to create a sustainable biomass-powered platform for PFOA degradation (Fig. 32d).[105] Oxygen-deficient CoFe alloy nanoparticles were anchored onto CNFs (CoFe-OVs@CNF), enabling dual-function cathodes (Fig. 32e). The toxicity evolution of degradation intermediates was evaluated, confirming the system's potential to degrade PFOA and other persistent pollutants while mitigating toxic risks (Fig. 32f).

To further expand the application scope of the SPEF system for PFAS degradation, Hou et al. developed a Cu-based peroxidase-mimicking colorimetric sensor integrated with an SPEF system for PFOA detection and removal (Fig. 33a).[106] The
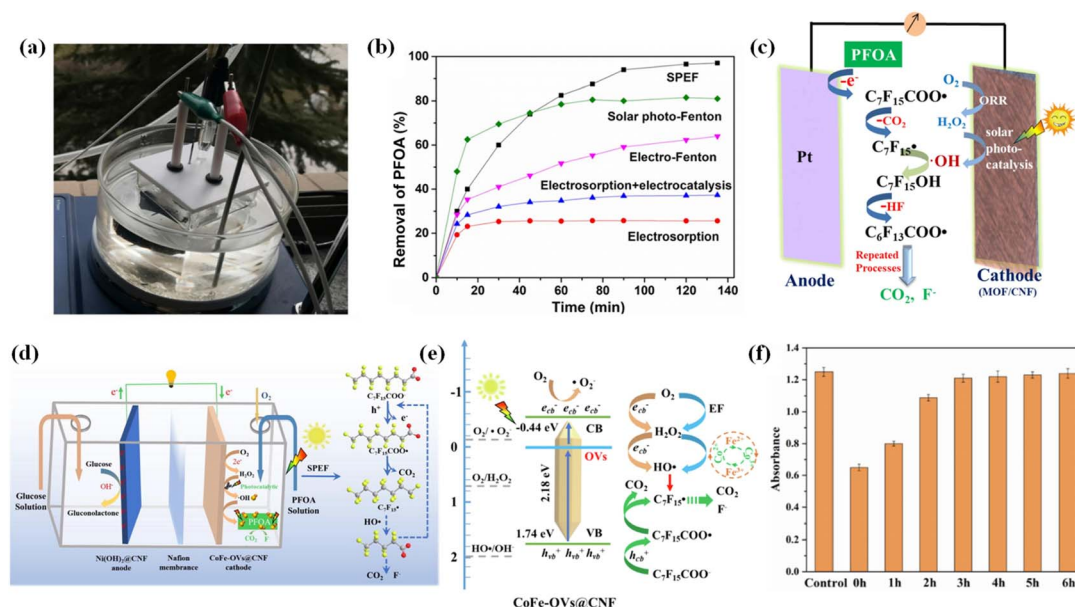
Fig. 32 (a) SPEF degradation of PFOA under outdoor natural sunlight conditions. (b) Removal of PFOA by SPEF, electro–Fenton, electrocatalysis and electrosorption, and electrosorption was conducted under N$_2$. (c) Mechanism of PFOA mineralization by the MOF/CNF constructed SPEF system.[104] (d) Glucose fuel cell driven SPEF process for the degradation of PFOA. (e) Proposed mechanism of the solar–photocatalytic coupled electro-Fenton process for PFOA degradation in the GFC–SPEF system. (f) MTT assay for the cell viability of L-02 cells incubated with PFOA over various degradation times (0–6 h).[105]

© 2026 The Author(s). Published by the Royal Society of Chemistry

Environ. Sci.: Adv., 2026, **5**, 9–42 | 33
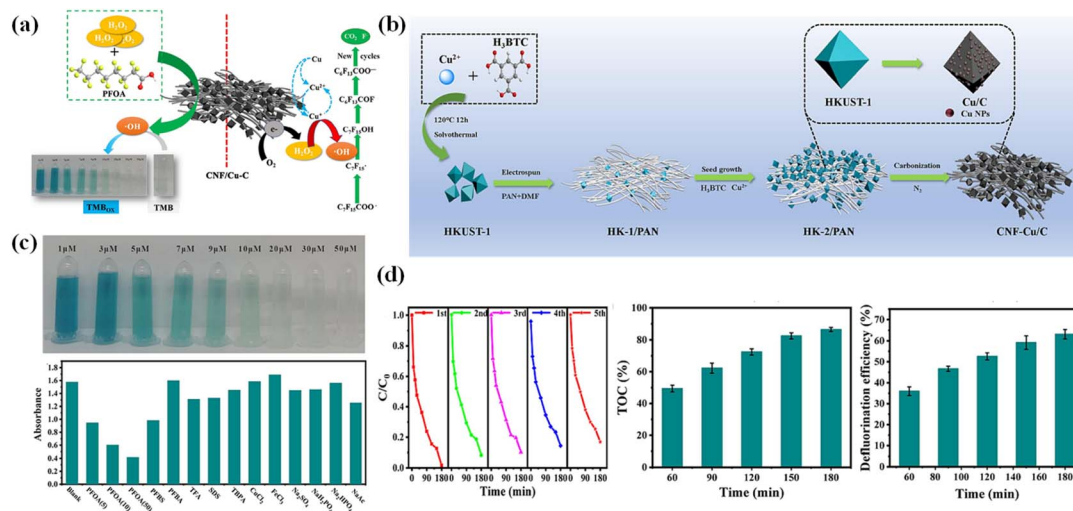
Fig. 33 (a) Schematic illustration of PFOA degradation *via* a MOF-derived Cu/carbon membrane. (b) Schematic diagram demonstration of the preparation of CNF-Cu/C. (c) Corresponding photographs for the colorimetric detection of PFOA (top) and selectivity of PFOA with other interfering substances (bottom). (d) Degradation rates under different conditions: reusability tests of CNF-Cu/C-800 in SPEF (left), TOC removal efficiency (mid), and defluorination efficiency (right).[106]

flexible, freestanding CNF-Cu/C membrane was synthesized *via* solvothermal processing, secondary seeding, and *in situ* thermal reduction (Fig. 33b). Derived from MOF/PAN precursors, the resulting 3D carbon network exhibited excellent conductivity, dispersion, and cycling stability (Fig. 33d). The CNF-Cu/C membrane showed strong peroxidase-like activity and enabled rapid PFOA detection *via* inhibition of TMB chromogenic reactions (Fig. 33c), with a detection limit of 0.133 μM. Under

optimized conditions, the Cu-SPEF system achieved 98% PFOA removal within 180 minutes. This work illustrates a successful integration of SPEF degradation and real-time detection, with significant practical potential.

In order to further elucidate the relationship between the structural characteristics of catalytic materials and PFAS degradation efficiency in SPEF systems, Hou *et al.* designed two-dimensional layered MOF-based CoFe nanosheets as

Fig. 34 (a) The preparation process of the 2D CoFe-OVs@NADE cathode and the construction process of the SPEF system. (b) The density of states in 2D CoFe-OVs. (c) The adsorption energy between PFOA and the two materials. (d) Mechanism of solar-photocatalytic coupled EF process for PFOA degradation in the SPEF system. (e) The effect of coexisting substances in the SPEF system.[107]

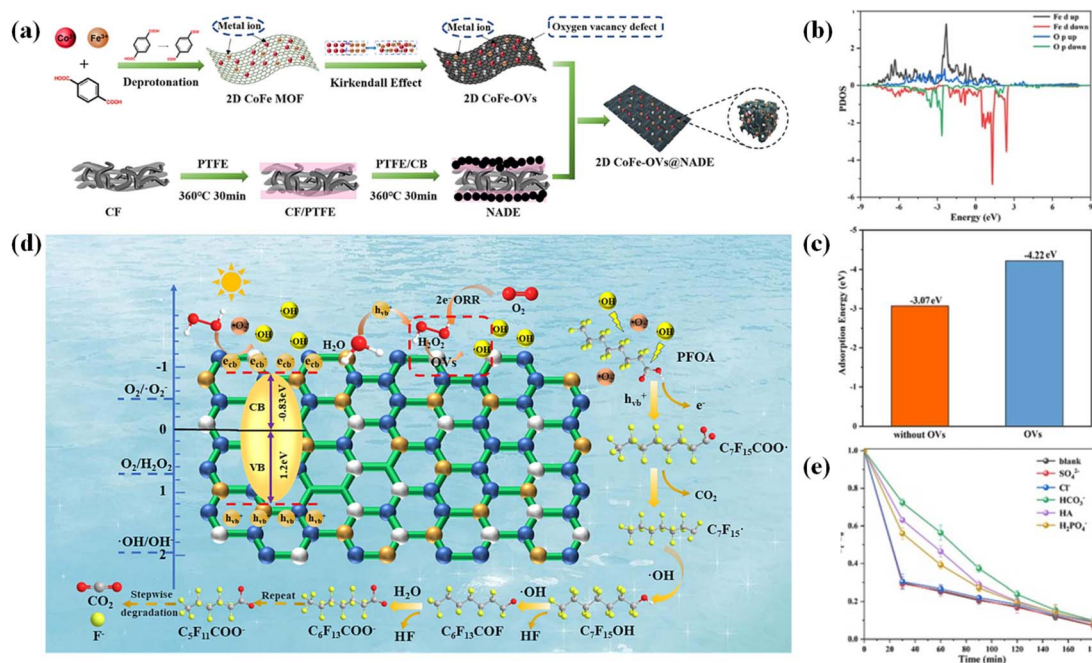photoelectrocatalysts.[107] The material featured abundant unsaturated coordination sites, which facilitated rapid mass and charge transport (Fig. 34a). Notably, low-temperature synthesis introduced oxygen vacancies (OVs) that modulated orbital interactions between Fe d-bands and O LUMO states, enhancing PFOA adsorption and reactivity (Fig. 34b and c). These OVs reduced the bandgap and improved charge separation, significantly boosting photoelectrocatalytic performance (Fig. 34d). The catalyst achieved effective degradation even in complex ionic matrices and real water samples (Fig. 34e), advancing the practical applicability of SPEF systems and deepening mechanistic understanding at the molecular interface.

The solar photo-electro-Fenton (SPEF) system integrates the advantages of both photo-Fenton and electro-Fenton processes by utilizing solar energy as a sustainable light source to generate photogenerated holes for PFAS activation, while simultaneously enabling the *in situ* generation of H_2O_2 and maintaining a stable Fe^{2+}/Fe^{3+} redox cycle inherent to electro-Fenton systems. This allows for efficient and environmentally friendly PFAS degradation without the need for external H_2O_2 addition. Moreover, SPEF systems can be coupled with colorimetric reactions to develop highly sensitive, real-time detection platforms for PFASs, highlighting their significant potential for future applications. However, the development of SPEF faces considerable challenges. Due to the complexity of the integrated system, there are stringent requirements for the structural design of materials used within the reaction framework. Achieving optimal performance demands materials that can simultaneously fulfill the distinct requirements of both photo-Fenton and electro-Fenton processes, which remains one of the most critical barriers to the broader application of SPEF technologies.

4. Summary and outlook

The degradation of PFASs is inherently challenging due to the high bond dissociation energy of C–F bonds, which requires not only large quantities of ˙OH but also effective activation of PFAS molecules to form reactive $˙C_nF_{2n+1}$ intermediates. Fenton reactions, owing to their ability to stably generate ˙OH, naturally emerged as a leading strategy. However, ˙OH alone is often insufficient to initiate PFAS activation. To overcome this limitation, multiple innovative approaches have been proposed.

Recent advances in Fenton-based strategies for PFAS degradation have been systematically summarized (Table 1), providing a more intuitive comparison of the relationships among reaction systems, operating conditions, and degradation efficiencies. Distinct reaction systems rely on different oxidative reactive species, which in turn lead to significant variations in PFAS degradation behaviors. In traditional Fenton systems, various radical precursors have been introduced to promote synergistic radical generation for enhanced PFAS degradation. Alternatively, spatial confinement strategies have been employed to restrict PFAS and ˙OH interactions within confined catalytic environments, thereby increasing the local radical concentration and reactivity. Additionally, several physical techniques—including electro-Fenton, photo-Fenton, and

SPEF—have been developed to facilitate PFAS activation through direct oxidation or electron–hole transfer, thereby enhancing coupling with ˙OH and subsequent defluorination steps. These hybrid methods not only circumvent the limitations of chemical Fenton systems, such as excessive H_2O_2 requirements, poor catalyst stability, and strict pH conditions, but also open up new possibilities for the sustainable treatment of PFASs. However, these advancements come with new challenges—particularly in the rational design of catalytic systems that can meet multiple performance criteria.

Considerable research efforts are still required to fully understand and optimize Fenton-based PFAS degradation. Continued exploration of Fenton-derived AOPs is essential to broaden the scope of PFAS treatment and to proactively address the challenges posed by emerging PFAS variants in future environmental scenarios. Among these developments, multi-strategy coupled Fenton systems, such as the recently proposed SPEF process, are regarded as some of the most promising approaches. By integrating multiple mechanisms, these systems can overcome the limitations inherent to individual methods. However, such integration also significantly increases the complexity of system design and material engineering. Based on the content of this review, the following research gaps and perspectives are proposed:

(1) Most existing studies have focused on the degradation of PFOA and PFOS, which are typically present at the highest concentrations in contaminated water. However, the PFAS concentrations ($\sim$10–50 mg L^{-1}) used in laboratory-scale experiments are far higher than those typically found in natural waters. Therefore, future research should focus on low-concentration PFAS degradation under environmentally relevant conditions to better meet real-world treatment demands.

(2) Current Fenton-based degradation systems have been primarily developed for PFOA, whereas studies on other PFAS species with diverse functional groups or backbone structures remain limited. Expanding the applicability of Fenton reactions to a broader range of PFASs is therefore an important direction for future research. Moreover, the influences of PFAS functional groups, backbone architectures, and spatial conformations on the degradation efficiency, degradation pathways, and byproduct formation in Fenton-based systems require further systematic investigation.

(3) Although novel Fenton-based systems have shown impressive performance, achieving over 95% PFAS degradation within a few hours, the formation of diverse transformation products—including short-chain intermediates, functional group modifications, and possible backbone alterations—remains a major concern. The limited identification of these byproducts and the lack of a comprehensive toxicological assessment raise the risk of secondary pollution. Addressing this challenge calls for integrated, multidisciplinary frameworks that link degradation efficiency with systematic analyses of byproduct formation, toxicity, and environmental fate. Future research should therefore move beyond removal rates toward holistic evaluations that ensure both treatment effectiveness and long-term environmental and biological safety.

© 2026 The Author(s). Published by the Royal Society of Chemistry

Environ. Sci.: Adv., 2026, **5**, 9–42 | **35**

Table 1 Recent studies on the degradation of PFASs by Fenton reactions

Catalysts	Target PFAS	$[PFAS]_0$	Experimental conditions	Degradation	Defluorination	Oxidant reactive species	Ref.
Chemical-Fenton reaction							
ZVI	PFOA	100 mg L^{-1}	ZVI (3.6 mM); PS (5.0 mM); 90 °C; microwave irradiation	68%	23%	$SO_4^{\cdot-}$ and $^{\cdot}OH$	80
Fe(III)	PFOA	100 μg L^{-1}	Fe(III) (0.5 mM); H$_2$O$_2$ (1.0 M); pH = 3.5; 20 °C	89%	—	$^{\cdot}OH$, $O_2^{\cdot-}$ and $HO_2^{\cdot}$	81
MD	PFOA	10 mg L^{-1}	HP (0.5 M); PS (0.3 M); MD (0.5 g in 60 mL solution); pH = 9.0	69%	—	$SO_4^{\cdot-}$, $^{\cdot}OH$ and $O_2^{\cdot-}$	82
Pb-BFO/rGO	PFOA	50 mg L^{-1}	Pb-BFO/rGO (1.0 g L^{-1}); H$_2$O$_2$ (44.0 mg L^{-1}); microwave (300.0 W); 5.0 min	95%	—	$^{\cdot}OH$	83
PGFe	PFOA	50 mg L^{-1}	PGFe (1.0 g L^{-1}); H$_2$O$_2$ (15.0 mM); pH = 6.0; 25 °C	22%	—	$^{\cdot}OH$	85
FeOCl	PFOA	20 mg L^{-1}	FeOCl (1.0 g L^{-1}); H$_2$O$_2$ (2.0 mM); pH = 5.2	57%	—	$^{\cdot}OH$ and $O_2^{\cdot-}$	86
HA	PFOA	41 mg L^{-1}	HA (600.0 mg L^{-1}); H$_2$O$_2$ (165 mM); Fe^{3+} (3 mM); pH = 3.0	100%	—	$^{\cdot}OH$	87
Electro-Fenton reaction							
Fe10MnC	PFOA	50 mg L^{-1}	Fe10MnC as the cathode and BDD as the anode; O$_2$ (100 mL min^{-1}); Na$_2$SO$_4$ as the electrolyte; pH = 3; j = 2.85 mA cm^{-2}	97%	—	$^{\cdot}OH$	88
FexNiC	PFOA	50 mg L^{-1}	FexNiC as cathodes, graphite sheet as the anode; O$_2$ (100 mL min^{-1}); KHSO$_5$ (40 mM); pH = 3.0; I = 25 mA	81%	—	$SO_4^{\cdot-}$ and $^{\cdot}OH$	89
Co-CN$_2$-Fe$_2$O$_3$	PFOA	10 mg L^{-1}	Co-CN$_2$-Fe$_2$O$_3$ as cathodes, Pt as the anode; O$_2$ (10 mL min^{-1}); Na$_2$SO$_4$ (0.05 M); pH = 2; V = −0.06 V	96%	96%	$^{\cdot}OH$	90
Fe/N-GE@GF	PFOA	20 mg L^{-1}	Fe/N-GE@GF as cathodes, DSA as the anode; Na$_2$SO$_4$ (0.05 M); pH = 7	95%	80%	$^{\cdot}OH$	91
F-NSGC	GenX	20 mg L^{-1}	F-NSGC as cathodes, Pt as the anode; Na$_2$SO$_4$ (0.05 M); pH = 3	96%	63%	$^{\cdot}OH$	92
Photo-Fenton reaction							
Fe(II)	PFOA	8 mg L^{-1}	Fe(II) (2.0 mM); H$_2$O$_2$ (30.0 mM); pH = 3.0; UV lamp (9 W)	95%	53%	$^{\cdot}OH$	94
Fe(III)	PFOA	20 mg L^{-1}	Fe(III) (1 mM); H$_2$O$_2$ (2.0 mM); UV light (4 W)	98%	13%	$^{\cdot}OH$	95
Fe^0/GAC	PFOA	50 mg L^{-1}	Fe^0 (7.5 g L^{-1}); GAC (12.5 g L^{-1}); H$_2$O$_2$ (22.8 mM); pH = 3; VUV light	—	47%	$^{\cdot}OH$	96
TiO$_2$-rGO	PFOA	10 mg L^{-1}	TiO$_2$-rGO (0.1 g L^{-1}); pH = 3.8; Hg lamp	93%	98%	$^{\cdot}OH$ and $O_2^{\cdot-}$	97

Table 1 (*Contd.*)

Catalysts	Target PFAS	$[PFAS]_0$	Experimental conditions	Degradation	Defluorination	Oxidant reactive species	Ref.
$Co_3O_4@Fe_3O_4$	PFOA	$20\ mg\ L^{-1}$	$Co_3O_4@Fe_3O_4$/cellulose as the membrane; H_2O_2 (30 mM); pH = 3; xenon lamp (300 W)	95%	—	$^{\cdot}OH$ and O_2^{-}	98
Fe-MMT	PFOA	$10\ mg\ L^{-1}$	Fe-MMT ($1.0\ g\ L^{-1}$); $HClO_4$ (0.1 M); pH = 3; Hg lamp (36 W)	90%	—	$^{\cdot}OH$ and O_2^{-}	100
DBD/FSB	PFOA	$20\ mg\ L^{-1}$	FSB ($100\ mg\ L^{-1}$); pH = 4.28; 22 kV peak voltage	93%	32%	$^{\cdot}OH$	102
GO-TiO₂	PFOS	$250\ \mu g\ L^{-1}$	$NaClO_4$ (50 mM); pH = 5.64; j = 20 mA cm^{-2}	99%	20%	$^{\cdot}OH$ and O_2^{-}	103
MOF/CNF	PFOA	$20\ mg\ L^{-1}$	Na_2SO_4 (50 mM); pH = 3; V = −0.6 V	99%	59%	$^{\cdot}OH$	104
CoFe-OVs@CNF	PFOA	$20\ mg\ L^{-1}$	Na_2SO_4 (50 mM); pH = 3; O₂ purge; xenon lamp (300 W)	95%	70%	$^{\cdot}OH$ and O_2^{-}	105
CNF-Cu/C	PFOA	$20\ mg\ L^{-1}$	Na_2SO_4 (50 mM); pH = 3; O₂ purge; xenon lamp (300 W)	98%	63%	$^{\cdot}OH$, O_2^{-} and HO_2^{-}	106
CoFe-OVs@NADE	PFOA	$20\ mg\ L^{-1}$	Na_2SO_4 (0.5 M); pH = 3; O₂ purge; xenon lamp (300 W)	93%	67%	$^{\cdot}OH$ and O_2^{-}	107

Section grouping: Solar photo-electro-Fenton system (DBD/FSB through CoFe-OVs@NADE).

(4) The development of increasingly sophisticated multi-method coupled Fenton systems presents considerable challenges for catalyst design and material selection. Future work should aim to elucidate the structure–activity relationships between catalyst composition and PFAS degradation performance. Establishing general design principles will enable the development of more effective catalytic materials specifically tailored for PFAS treatment.

(5) Despite widespread attention to Fenton-based AOPs for PFAS degradation, their performance in complex environmental waters has not been systematically evaluated. Moreover, current Fenton systems typically operate at relatively small treatment volumes. Large-scale water treatment applications require comprehensive studies of process scalability and techno-economic performance. In this context, life cycle assessment (LCA) and techno-economic analysis (TEA) should be considered in future evaluations of PFAS treatment technologies.

Author contributions

Zhicong Huang: conceptualization; data curation; visualization; validation; writing – original draft; writing – review & editing. Xi Huang: investigation. Kang Liu: supervision. Junwei Fu: conceptualization; funding acquisition; project administration; resources; supervision; writing – review & editing. Min Liu: supervision.

Conflicts of interest

The authors declare that they have no known competing financial interests or personal relationships that could have appeared to influence the work reported in this paper.

Data availability

No primary research results, software or code have been included and no new data were generated or analysed as part of this review.

Acknowledgements

References

1 H. Li, A. L. Junker, J. Wen, L. Ahrens, M. Sillanpää, J. Tian, F. Cui, L. Vergeynst and Z. Wei, A recent overview of per- and polyfluoroalkyl substances (PFAS) removal by functional framework materials, *Chem. Eng. J.*, 2023, **452**, 139202.

2 Y. Li, Z. Niu and Y. Zhang, Occurrence of legacy and emerging poly- and perfluoroalkyl substances in water: A

case study in Tianjin (China), *Chemosphere*, 2022, **287**, 132409.

3 K. Kannan, Perfluoroalkyl and polyfluoroalkyl substances: current and future perspectives, *Environ. Chem.*, 2011, **8**, 333.

4 N. Chowdhury, S. Prabakar and H. Choi, Dependency of the photocatalytic and photochemical decomposition of per- and polyfluoroalkyl substances (PFAS) on their chain lengths, functional groups, and structural properties, *Water Sci. Technol.*, 2021, **84**, 3738–3754.

5 F. Li, J. Duan, S. Tian, H. Ji, Y. Zhu, Z. Wei and D. Zhao, Short-chain per- and polyfluoroalkyl substances in aquatic systems: Occurrence, impacts and treatment, *Chem. Eng. J.*, 2020, **380**, 122506.

6 J. John, F. Coulon and P. V. Chellam, Detection and treatment strategies of per- and polyfluoroalkyl substances (PFAS): Fate of PFAS through DPSIR framework analysis, *J. Water Process Eng.*, 2022, **45**, 102463.

7 S. Garg, J. Wang, P. Kumar, V. Mishra, H. Arafat, R. S. Sharma and L. F. Dumée, Remediation of water from per-/poly-fluoroalkyl substances (PFAS) – Challenges and perspectives, *J. Environ. Chem. Eng.*, 2021, **9**, 105784.

8 J. P. Giesy and K. Kannan, Peer Reviewed: Perfluorochemical Surfactants in the Environment, *Environ. Sci. Technol.*, 2002, **36**, 146A–152A.

9 B. D. Key, R. D. Howell and C. S. Criddle, Fluorinated Organics in the Biosphere, *Environ. Sci. Technol.*, 1997, **31**, 2445–2454.

10 M. Kotthoff, J. Muller, H. Jurling, M. Schlummer and D. Fiedler, Perfluoroalkyl and polyfluoroalkyl substances in consumer products, *Environ. Sci. Pollut. Res. Int.*, 2015, **22**, 14546–14559.

11 D. R. Taves, Evidence that there are Two Forms of Fluoride in Human Serum, *Nature*, 1968, **217**, 1050–1051.

12 C. G. Pan, S. K. Xiao, K. F. Yu, Q. Wu and Y. H. Wang, Legacy and alternative per- and polyfluoroalkyl substances in a subtropical marine food web from the Beibu Gulf, South China: Fate, trophic transfer and health risk assessment, *J. Hazard. Mater.*, 2021, **403**, 123618.

13 X. Liang, J. Zhou, X. Yang, W. Jiao, T. Wang and L. Zhu, Disclosing the bioaccumulation and biomagnification behaviors of emerging per/polyfluoroalkyl substances in aquatic food web based on field investigation and model simulation, *J. Hazard. Mater.*, 2023, **445**, 130566.

14 S. Yi, P. Chen, L. Yang and L. Zhu, Probing the hepatotoxicity mechanisms of novel chlorinated polyfluoroalkyl sulfonates to zebrafish larvae: Implication of structural specificity, *Environ. Int.*, 2019, **133**, 105262.

15 A. Hagenaars, D. Knapen, I. J. Meyer, K. van der Ven, P. Hoff and W. De Coen, Toxicity evaluation of perfluorooctane sulfonate (PFOS) in the liver of common carp (Cyprinus carpio), *Aquat. Toxicol.*, 2008, **88**, 155–163.

16 K. Li, P. Gao, P. Xiang, X. Zhang, X. Cui and L. Q. Ma, Molecular mechanisms of PFOA-induced toxicity in animals and humans: Implications for health risks, *Environ. Int.*, 2017, **99**, 43–54.

17 M. Liu, S. Yi, H. Yu, T. Zhang, F. Dong and L. Zhu, Underlying Mechanisms for the Sex- and Chemical-Specific Hepatotoxicity of Perfluoroalkyl Phosphinic Acids in Common Carp (Cyprinus carpio), *Environ. Sci. Technol.*, 2023, **57**, 14515–14525.

18 S. Yi, J. Wang, R. Wang, M. Liu, W. Zhong, L. Zhu and G. Jiang, Structure-Related Thyroid Disrupting Effect of Perfluorooctanesulfonate-like Substances in Zebrafish Larvae, *Environ. Sci. Technol.*, 2024, **58**, 182–193.

19 J. Guo, J. Zhou, S. Liu, L. Shen, X. Liang, T. Wang and L. Zhu, Underlying Mechanisms for Low-Molecular-Weight Dissolved Organic Matter to Promote Translocation and Transformation of Chlorinated Polyfluoroalkyl Ether Sulfonate in Wheat, *Environ. Sci. Technol.*, 2022, **56**, 15617–15626.

20 S. Liu, J. Zhou, J. Guo, M. Xue, L. Shen, S. Bai, X. Liang, T. Wang and L. Zhu, Impact Mechanisms of Humic Acid on the Transmembrane Transport of Per- and Polyfluoroalkyl Substances in Wheat at the Subcellular Level: The Important Role of Slow-Type Anion Channels, *Environ. Sci. Technol.*, 2023, **57**, 8739–8749.

21 X. Yang, C. Ye, Y. Liu and F. J. Zhao, Accumulation and phytotoxicity of perfluorooctanoic acid in the model plant species Arabidopsis thaliana, *Environ. Pollut.*, 2015, **206**, 560–566.

22 L. Fan, J. Tang, D. Zhang, M. Ma, Y. Wang and Y. Han, Investigations on the phytotoxicity of perfluorooctanoic acid in Arabidopsis thaliana, *Environ. Sci. Pollut. Res. Int.*, 2020, **27**, 1131–1143.

23 Q. Guo, Z. He, X. Liu, B. Liu and Y. Zhang, High-throughput non-targeted metabolomics study of the effects of perfluorooctane sulfonate (PFOS) on the metabolic characteristics of A. thaliana leaves, *Sci. Total Environ.*, 2020, **710**, 135542.

24 P. Li, X. Oyang, X. Xie, Z. Li, H. Yang, J. Xi, Y. Guo, X. Tian, B. Liu, J. Li and Z. Xiao, Phytotoxicity induced by perfluorooctanoic acid and perfluorooctane sulfonate via metabolomics, *J. Hazard. Mater.*, 2020, **389**, 121852.

25 P. Li, J. Sun, X. Xie, Z. Li, B. Huang, G. Zhang, J. Li and Z. Xiao, Stress response and tolerance to perfluorooctane sulfonate (PFOS) in lettuce (Lactuca sativa), *J. Hazard. Mater.*, 2021, **404**, 124213.

26 F. Chi, S. Zhao, L. Yang, X. Yang, X. Zhao, R. Zhao, L. Zhu and J. Zhan, Unveiling behaviors of 8:2 fluorotelomer sulfonic acid (8:2 FTSA) in Arabidopsis thaliana: Bioaccumulation, biotransformation and molecular mechanisms of phytotoxicity, *Sci. Total Environ.*, 2024, **927**, 172165.

27 S. E. Fenton, A. Ducatman, A. Boobis, J. C. DeWitt, C. Lau, C. Ng, J. S. Smith and S. M. Roberts, Per- and Polyfluoroalkyl Substance Toxicity and Human Health Review: Current State of Knowledge and Strategies for Informing Future Research, *Environ. Toxicol. Chem.*, 2021, **40**, 606–630.

28 Y. Zhu, X. Yang, X. Song, Y. Jia, Y. Zhang and L. Zhu, Insights into the Enhanced Bioavailability of Per- and Polyfluoroalkyl Substances in Food Caused by Chronic

Inflammatory Bowel Disease, *Environ. Sci. Technol.*, 2024, **58**, 11912–11922.

29 Q. Chen, S. Yi, Y. Sun, Y. Zhu, K. Ma and L. Zhu, Contribution of Continued Dermal Exposure of PFAS-Containing Sunscreens to Internal Exposure: Extrapolation from In Vitro and In Vivo Tests to Physiologically Based Toxicokinetic Models, *Environ. Sci. Technol.*, 2024, **58**, 15005–15016.

30 J. F. C. Glatz and J. Luiken, Dynamic role of the transmembrane glycoprotein CD36 (SR-B2) in cellular fatty acid uptake and utilization, *J. Lipid Res.*, 2018, **59**, 1084–1093.

31 Y. Jia, Y. Zhu, R. Wang, Q. Ye, D. Xu, W. Zhang, Y. Zhang, G. Shan and L. Zhu, Novel insights into the mediating roles of cluster of differentiation 36 in transmembrane transport and tissue partition of per- and polyfluoroalkyl substances in mice, *J. Hazard. Mater.*, 2023, **442**, 130129.

32 U. S. E. P. Agency, Interim Updated PFOA and PFOS Health Advisories, Available online: **https://www.epa.gov/sdwa/drinking-water-health-advisories-pfoa-and-pfos** (accessed on 15 June 2022).

33 Eurofins, *PFAS in the Revised Drinking Water Directive (DWD)*, Available online: **https://eur-lex.europa.eu/eli/C/2024/4910/oj/**, (accessed on 26 May 2023).

34 L. Liu, Y. Qu, J. Huang and R. Weber, Per- and polyfluoroalkyl substances (PFASs) in Chinese drinking water: risk assessment and geographical distribution, *Environ. Sci. Eur.*, 2021, **33**, 6–17.

35 K. Y. Tan, G. H. Lu, H. T. Piao, S. Chen, X. C. Jiao, N. Gai, E. Yamazaki, N. Yamashita, J. Pan and Y. L. Yang, Current Contamination Status of Perfluoroalkyl Substances in Tapwater from 17 Cities in the Eastern China and Their Correlations with Surface Waters, *Bull. Environ. Contam. Toxicol.*, 2017, **99**, 224–231.

36 H. Yin, R. Chen, H. Wang, C. Schwarz, H. Hu, B. Shi and Y. Wang, Co-occurrence of phthalate esters and perfluoroalkyl substances affected bacterial community and pathogenic bacteria growth in rural drinking water distribution systems, *Sci. Total Environ.*, 2023, **856**, 158943.

37 H. Park, G. Choo, H. Kim and J. E. Oh, Evaluation of the current contamination status of PFASs and OPFRs in South Korean tap water associated with its origin, *Sci. Total Environ.*, 2018, **634**, 1505–1512.

38 K. Y. Kim, O. D. Ekpe, H. J. Lee and J. E. Oh, Perfluoroalkyl substances and pharmaceuticals removal in full-scale drinking water treatment plants, *J. Hazard. Mater.*, 2020, **400**, 123235.

39 M. Babayev, S. L. Capozzi, P. Miller, K. R. McLaughlin, S. S. Medina, S. Byrne, G. Zheng and A. Salamova, PFAS in drinking water and serum of the people of a southeast Alaska community: A pilot study, *Environ. Pollut.*, 2022, **305**, 119246.

40 C. S. Skaggs and B. A. Logue, Ultratrace analysis of per- and polyfluoroalkyl substances in drinking water using ice concentration linked with extractive stirrer and high performance liquid chromatography – tandem mass spectrometry, *J. Chromatogr. A*, 2021, **1659**, 462493.

41 K. Arinaitwe, N. Keltsch, A. Taabu-Munyaho, T. Reemtsma and U. Berger, Perfluoroalkyl substances (PFASs) in the Ugandan waters of Lake Victoria: Spatial distribution, catchment release and public exposure risk via municipal water consumption, *Sci. Total Environ.*, 2021, **783**, 146970.

42 Y. Liu, X. Li, X. Wang, X. Qiao, S. Hao, J. Lu, X. Duan, D. D. Dionysiou and B. Zheng, Contamination Profiles of Perfluoroalkyl Substances (PFAS) in Groundwater in the Alluvial-Pluvial Plain of Hutuo River, China, *Water*, 2019, **11**, 1–2316.

43 M. A. Petre, D. P. Genereux, L. Koropeckyj-Cox, D. R. U. Knappe, S. Duboscq, T. E. Gilmore and Z. R. Hopkins, Per- and Polyfluoroalkyl Substance (PFAS) Transport from Groundwater to Streams near a PFAS Manufacturing Facility in North Carolina, USA, *Environ. Sci. Technol.*, 2021, **55**, 5848–5856.

44 A. Wagner, B. Raue, H. J. Brauch, E. Worch and F. T. Lange, Determination of adsorbable organic fluorine from aqueous environmental samples by adsorption to polystyrene-divinylbenzene based activated carbon and combustion ion chromatography, *J. Chromatogr. A*, 2013, **1295**, 82–89.

45 L. Gobelius, J. Hedlund, W. Durig, R. Troger, K. Lilja, K. Wiberg and L. Ahrens, Per- and Polyfluoroalkyl Substances in Swedish Groundwater and Surface Water: Implications for Environmental Quality Standards and Drinking Water Guidelines, *Environ. Sci. Technol.*, 2018, **52**, 4340–4349.

46 S. Banzhaf, M. Filipovic, J. Lewis, C. J. Sparrenbom and R. Barthel, A review of contamination of surface-, ground-, and drinking water in Sweden by perfluoroalkyl and polyfluoroalkyl substances (PFASs), *Ambio*, 2017, **46**, 335–346.

47 M. Filipovic, A. Woldegiorgis, K. Norstrom, M. Bibi, M. Lindberg and A. H. Osteras, Historical usage of aqueous film forming foam: a case study of the widespread distribution of perfluoroalkyl acids from a military airport to groundwater, lakes, soils and fish, *Chemosphere*, 2015, **129**, 39–45.

48 E. Hepburn, C. Madden, D. Szabo, T. L. Coggan, B. Clarke and M. Currell, Contamination of groundwater with per- and polyfluoroalkyl substances (PFAS) from legacy landfills in an urban re-development precinct, *Environ. Pollut.*, 2019, **248**, 101–113.

49 D. Szabo, T. L. Coggan, T. C. Robson, M. Currell and B. O. Clarke, Investigating recycled water use as a diffuse source of per- and polyfluoroalkyl substances (PFASs) to groundwater in Melbourne, Australia, *Sci. Total Environ.*, 2018, **644**, 1409–1417.

50 X. Song, R. Vestergren, Y. Shi, J. Huang and Y. Cai, Emissions, Transport, and Fate of Emerging Per- and Polyfluoroalkyl Substances from One of the Major Fluoropolymer Manufacturing Facilities in China, *Environ. Sci. Technol.*, 2018, **52**, 9694–9703.

51 H.-C. Wang, T.-H. Yeo, S. Nobarany and G. Hsieh, *Presented in Part at the Proceedings of the Third International Symposium of Chinese CHI*, 2015.

© 2026 The Author(s). Published by the Royal Society of Chemistry

Environ. Sci.: Adv., 2026, **5**, 9–42 | 39

52 Y. Pan, H. Zhang, Q. Cui, N. Sheng, L. W. Y. Yeung, Y. Sun, Y. Guo and J. Dai, Worldwide Distribution of Novel Perfluoroether Carboxylic and Sulfonic Acids in Surface Water, *Environ. Sci. Technol.*, 2018, **52**, 7621–7629.

53 Y. Zhang, R. Dong, F. Ge, M. Hong, Z. Chen, Y. Zhou, J. Wei, C. Gu and D. Kong, Removal of 48 per- and polyfluoroalkyl substances (PFAS) throughout processes in domestic and general industrial wastewater treatment plants: Implications for emerging alternatives risk control, *J. Hazard. Mater.*, 2024, **480**, 136130.

54 K. Y. Kim, M. Ndabambi, S. Choi and J. E. Oh, Legacy and novel perfluoroalkyl and polyfluoroalkyl substances in industrial wastewater and the receiving river water: Temporal changes in relative abundances of regulated compounds and alternatives, *Water Res.*, 2021, **191**, 116830.

55 X. Dauchy, V. Boiteux, C. Bach, A. Colin, J. Hemard, C. Rosin and J. F. Munoz, Mass flows and fate of per- and polyfluoroalkyl substances (PFASs) in the wastewater treatment plant of a fluorochemical manufacturing facility, *Sci. Total Environ.*, 2017, **576**, 549–558.

56 S. Huang, M. Sima, Y. Long, C. Messenger and P. R. Jaffe, Anaerobic degradation of perfluorooctanoic acid (PFOA) in biosolids by Acidimicrobium sp. strain A6, *J. Hazard. Mater.*, 2022, **424**, 127699.

57 S. Wang, T. Liu, X. Qian, H. Wang, M. Li, X. Wang, S. Wei and H. Chen, Microbial plankton responses to perfluoroalkyl acids and their alternatives in the aquatic environment, *J. Hazard. Mater.*, 2023, **441**, 129980.

58 Y. Huang, W. Zhang, M. Bai and X. Huang, One-pot fabrication of magnetic fluorinated carbon nanotubes adsorbent for efficient extraction of perfluoroalkyl carboxylic acids and perfluoroalkyl sulfonic acids in environmental water samples, *Chem. Eng. J.*, 2020, **380**, 122392.

59 G. Niarchos, L. Ahrens, D. B. Kleja and F. Fagerlund, Per- and polyfluoroalkyl substance (PFAS) retention by colloidal activated carbon (CAC) using dynamic column experiments, *Environ. Pollut.*, 2022, **308**, 119667.

60 T. A. Bruton and D. L. Sedlak, Treatment of Aqueous Film-Forming Foam by Heat-Activated Persulfate Under Conditions Representative of *In Situ* Chemical Oxidation, *Environ. Sci. Technol.*, 2017, **51**, 13878–13885.

61 Y. Bao, J. Huang, G. Cagnetta and G. Yu, Removal of F-53B as PFOS alternative in chrome plating wastewater by UV/Sulfite reduction, *Water Res.*, 2019, **163**, 114907.

62 J. Cui, P. Gao and Y. Deng, Destruction of Per- and Polyfluoroalkyl Substances (PFAS) with Advanced Reduction Processes (ARPs): A Critical Review, *Environ. Sci. Technol.*, 2020, **54**, 3752–3766.

63 M. Pierpaoli, M. Szopinska, B. K. Wilk, M. Sobaszek, A. Luczkiewicz, R. Bogdanowicz and S. Fudala-Ksiazek, Electrochemical oxidation of PFOA and PFOS in landfill leachates at low and highly boron-doped diamond electrodes, *J. Hazard. Mater.*, 2021, **403**, 123606.

64 L. P. Wackett, Why Is the Biodegradation of Polyfluorinated Compounds So Rare?, *mSphere*, 2021, **6**, e0072121.

65 W. H. Glaze, J.-W. Kang and D. H. Chapin, The Chemistry of Water Treatment Processes Involving Ozone, Hydrogen Peroxide and Ultraviolet Radiation, *Ozone: Sci. Eng.*, 1987, **9**, 335–352.

66 L. Yang, Y. Jiao, X. Xu, Y. Pan, C. Su, X. Duan, H. Sun, S. Liu, S. Wang and Z. Shao, Superstructures with Atomic-Level Arranged Perovskite and Oxide Layers for Advanced Oxidation with an Enhanced Non-Free Radical Pathway, *ACS Sustain. Chem. Eng.*, 2022, **10**, 1899–1909.

67 H. J. H. Fenton, LXXIII.—Oxidation of tartaric acid in presence of iron, *J. Chem. Soc., Trans.*, 1894, **65**, 899–910.

68 M. H. Zhang, H. Dong, L. Zhao, D. X. Wang and D. Meng, A review on Fenton process for organic wastewater treatment based on optimization perspective, *Sci. Total Environ.*, 2019, **670**, 110–121.

69 I. Mesquita, L. C. Matos, F. Duarte, F. J. Maldonado-Hodar, A. Mendes and L. M. Madeira, Treatment of azo dye-containing wastewater by a Fenton-like process in a continuous packed-bed reactor filled with activated carbon, *J. Hazard. Mater.*, 2012, **237–238**, 30–37.

70 F. Duarte, F. J. Maldonado-Hódar and L. M. Madeira, Influence of the characteristics of carbon materials on their behaviour as heterogeneous Fenton catalysts for the elimination of the azo dye Orange II from aqueous solutions, *Appl. Catal., B*, 2011, **103**, 109–115.

71 C. Kim, P. Debusmann, M. S. Abdighahroudi, J. Schumacher and H. V. Lutze, Fenton-coagulation process for simultaneous abatement of micropollutants and dissolved organic carbon in treated wastewater, *Water Res.*, 2025, **281**, 123583.

72 Z. Ye, E. Brillas, F. Centellas, P. L. Cabot and I. Sires, Expanding the application of photoelectro-Fenton treatment to urban wastewater using the Fe(III)-EDDS complex, *Water Res.*, 2020, **169**, 115219.

73 M. J. Chen, S. L. Lo, Y. C. Lee and C. C. Huang, Photocatalytic decomposition of perfluorooctanoic acid by transition-metal modified titanium dioxide, *J. Hazard. Mater.*, 2015, **288**, 168–175.

74 X. Dai, Z. Xie, B. Dorian, S. Gray and J. Zhang, Comparative study of PFAS treatment by UV, UV/ozone, and fractionations with air and ozonated air, *Environ. Sci.:Water Res. Technol.*, 2019, **5**, 1897–1907.

75 N. Duinslaeger and J. Radjenovic, Electrochemical degradation of per- and polyfluoroalkyl substances (PFAS) using low-cost graphene sponge electrodes, *Water Res.*, 2022, **213**, 118148.

76 B. Utset, J. Garcia, J. Casado, X. Domènech and J. Peral, Replacement of H_2O_2 by O_2 in Fenton and photo-Fenton reactions, *Chemosphere*, 2000, **41**, 1187–1192.

77 W. Song, M. Cheng, J. Ma, W. Ma, C. Chen and J. Zhao, Decomposition of Hydrogen Peroxide Driven by Photochemical Cycling of Iron Species in Clay, *Environ. Sci. Technol.*, 2006, **40**, 4782–4787.

78 M. L. Rodriguez, V. I. Timokhin, S. Contreras, E. Chamarro and S. Esplugas, Rate equation for the degradation of nitrobenzene by 'Fenton-like' reagent, *Adv. Environ. Res.*, 2003, **7**, 583–595.

79 J. J. Pignatello, E. Oliveros and A. MacKay, Advanced Oxidation Processes for Organic Contaminant Destruction Based on the Fenton Reaction and Related Chemistry, *Crit. Rev. Environ. Sci. Technol.*, 2006, **36**, 1–84.

80 Y. C. Lee, S. L. Lo, P. T. Chiueh, Y. H. Liou and M. L. Chen, Microwave-hydrothermal decomposition of perfluorooctanoic acid in water by iron-activated persulfate oxidation, *Water Res.*, 2010, **44**, 886–892.

81 S. M. Mitchell, M. Ahmad, A. L. Teel and R. J. Watts, Degradation of Perfluorooctanoic Acid by Reactive Species Generated through Catalyzed H_2O_2 Propagation Reactions, *Environ. Sci. Technol. Lett.*, 2013, **1**, 117–121.

82 C. K. O. da Silva-Rackov, W. A. Lawal, P. A. Nfodzo, M. M. G. R. Vianna, C. A. O. do Nascimento and H. Choi, Degradation of PFOA by hydrogen peroxide and persulfate activated by iron-modified diatomite, *Appl. Catal., B*, 2016, **192**, 253–259.

83 S. Li, G. Zhang, W. Zhang, H. Zheng, W. Zhu, N. Sun, Y. Zheng and P. Wang, Microwave enhanced Fenton-like process for degradation of perfluorooctanoic acid (PFOA) using Pb-$BiFeO_3$/rGO as heterogeneous catalyst, *Chem. Eng. J.*, 2017, **326**, 756–764.

84 Y. Zhuang, X. Wang, L. Zhang, Z. Kou and B. Shi, Confinement Fenton-like degradation of perfluorooctanoic acid by a three dimensional metal-free catalyst derived from waste, *Appl. Catal., B*, 2020, **275**, 119101.

85 X. Wang, Y. Zhuang, J. Zhang, L. Song and B. Shi, Pollutant degradation behaviors in a heterogeneous Fenton system through Fe/S-doped aerogel, *Sci. Total Environ.*, 2020, **714**, 136436.

86 J. Zheng and S. Zhang, Subnanoscale spatially confined heterogeneous Fenton reaction enables mineralization of perfluorooctanoic acid, *Water Res.*, 2023, **246**, 120696.

87 A. Santos, S. Rodriguez, F. Pardo and A. Romero, Use of Fenton reagent combined with humic acids for the removal of PFOA from contaminated water, *Sci. Total Environ.*, 2016, **563–564**, 657–663.

88 Q. Wang, M. Liu, H. Zhao, Y. Chen, F. Xiao, W. Chu and G. Zhao, Efficiently degradation of perfluorooctanoic acid in synergic electrochemical process combining cathodic electro-Fenton and anodic oxidation, *Chem. Eng. J.*, 2019, **378**, 122071.

89 Q. Lei, M. Liu, T. Yang, M. Chen, L. Qian, S. Mao, J. Cai and H. Zhao, Controllable Generation of Sulfate and Hydroxyl Radicals to Efficiently Degrade Perfluorooctanoic Acid in Cathode-Dominated Electrochemical Process, *ACS ES&T Water*, 2023, **3**, 3696–3707.

90 J. Han, M. Zhao, K. Wu, Y. Hong, T. Huang, X. Gu, Z. Wang, S. Liu and G. Zhu, A bifunctional single-atom catalyst assisted by Fe_2O_3 for efficiently electrocatalytic perfluorooctanoic acid degradation by integrating reductive and oxidative processes, *Chem. Eng. J.*, 2023, **470**, 144270.

91 F. Yu, Y. Zhang, Y. Zhang, Y. Gao and Y. Pan, Promotion of the degradation perfluorooctanoic acid by electro-Fenton under the bifunctional electrodes: Focusing active reaction region by Fe/N co-doped graphene modified cathode, *Chem. Eng. J.*, 2023, **457**, 141320.

92 Y. Wang, H. Li, J. Li, L. Zhou, C. Feng, G. Liu, J. Wang and C. Hou, Fluorophilic N, S self-doped porous carbon electrodes derived from biomass gelatin for electro-Fenton degradation of GenX, *J. Environ. Chem. Eng.*, 2025, **13**, 115386.

93 H. D. Hieu Nhu, D. V. Tri, T. L. Luu, J. Trippel and M. Wagner, Degradation of 29 per- and poly-fluoroalkyl substances (PFAS) in water using fenton-assisted electrochemical oxidation process, *Sep. Purif. Technol.*, 2025, **362**, 131908.

94 H. Tang, Q. Xiang, M. Lei, J. Yan, L. Zhu and J. Zou, Efficient degradation of perfluorooctanoic acid by UV–Fenton process, *Chem. Eng. J.*, 2012, **184**, 156–162.

95 D. Liu, Z. Xiu, F. Liu, G. Wu, D. Adamson, C. Newell, P. Vikesland, A. L. Tsai and P. J. Alvarez, Perfluorooctanoic acid degradation in the presence of Fe(III) under natural sunlight, *J. Hazard. Mater.*, 2013, **262**, 456–463.

96 L. H. Zhang, J. H. Cheng, X. You, X. Y. Liang and Y. Y. Hu, Photochemical defluorination of aqueous perfluorooctanoic acid (PFOA) by Fe(0)/GAC micro-electrolysis and VUV-Fenton photolysis, *Environ. Sci. Pollut. Res. Int.*, 2016, **23**, 13531–13542.

97 B. Gomez-Ruiz, P. Ribao, N. Diban, M. J. Rivero, I. Ortiz and A. Urtiaga, Photocatalytic degradation and mineralization of perfluorooctanoic acid (PFOA) using a composite TiO_2-rGO catalyst, *J. Hazard. Mater.*, 2018, **344**, 950–957.

98 J. Gao, W. Chen, H. Shi, Z. Li, L. Jing, C. Hou, J. Wang and Y. Wang, Co_3O_4@Fe_3O_4/cellulose blend membranes for efficient degradation of perfluorooctanoic acid in the visible light-driven photo-Fenton system, *Surf. Interfaces*, 2022, **34**, 102302.

99 P. Su, C. Zhang, Y. Liu, J. Zhang, R. Djellabi, R. Wang, J. Guo, R. Zhang, H. Guo, X. Ding and X. Liu, Boosting PFOA photocatalytic removal from water using highly adsorptive and sunlight-responsive ZIF67/MIL-100(Fe) modified C_3N_4, *J. Environ. Chem. Eng.*, 2023, **11**, 110765.

100 Y. Zhang, X. Wang, Y. Xu, L. Huang, W. Wang, C. Gu, M. Zhang and Z. Chen, Photochemical degradation of perfluorooctanoic acid under UV irradiation in the presence of Fe (III)-saturated montmorillonite, *Sci. Total Environ.*, 2023, **876**, 162760.

101 C. L. Quiroz-Vela, H. Zúñiga-Benítez and G. A. Peñuela, Application of photochemical treatments in the removal of perfluorooctanoic acid (PFOA) from aqueous solutions, *J. Environ. Chem. Eng.*, 2024, **12**, 112259.

102 L. Wang, L. Sun, Z. Yu, Y. Hou, Z. Peng, F. Yang, Y. Chen and J. Huang, Synergetic decomposition performance and mechanism of perfluorooctanoic acid in dielectric barrier discharge plasma system with Fe_3O_4@SiO_2-BiOBr magnetic photocatalyst, *Mol. Catal.*, 2017, **441**, 179–189.

103 J. S. Yang, W. W. Lai and A. Y. Lin, New insight into PFOS transformation pathways and the associated competitive inhibition with other perfluoroalkyl acids via

© 2026 The Author(s). Published by the Royal Society of Chemistry

Environ. Sci.: Adv., 2026, **5**, 9–42 | 41

photoelectrochemical processes using GOTiO$_2$ film photoelectrodes, *Water Res.*, 2021, **207**, 117805.

104 Y. Wang, M. Zhao, C. Hou, W. Chen, S. Li, R. Ren and Z. Li, Efficient degradation of perfluorooctanoic acid by solar photo-electro-Fenton like system fabricated by MOFs/ carbon nanofibers composite membrane, *Chem. Eng. J.*, 2021, **414**, 128940.

105 Y. Wang, S. Li, Y. Shao, L. Jing, R. Ren, L. Ma, X. Wang, Z. Li, J. Wang and C. Hou, Energy-efficient mineralization of perfluorooctanoic acid: Biomass energy driven solar photo-electro-fenton catalysis and mechanism study, *Chem. Eng. J.*, 2022, **443**, 136514.

106 C. Hou, F. Chen, D. Cheng, S. Zou, J. Wang, M. Shen and Y. Wang, MOFs-derived Cu/Carbon membrane as bi-functional catalyst: Improving catalytic activity in detection and degradation of PFOA via regulation of reactive Cu species, *Chem. Eng. J.*, 2024, **481**, 148467.

107 Y. Wang, Y. Chen, Q. Meng, J. Li, L. Jing, H. Li, L. Zhou, Z. Tian, J. Wang and C. Hou, Efficient photo-electro-Fenton catalysis of perfluorooctanoic acid with MOFs based 2D CoFe nanosheets: Oxygen vacancy-mediated adsorption and mineralization ability, *Chem. Eng. J.*, 2024, **483**, 149385.

108 H. Hori, E. Hayakawa, H. Einaga, S. Kutsuna, K. Koike, T. Ibusuki, H. Kiatagawa and R. Arakawa, Decomposition of Environmentally Persistent Perfluorooctanoic Acid in Water by Photochemical Approaches, *Environ. Sci. Technol.*, 2004, **38**, 6118–6124.

109 H. Moriwaki, Y. Takagi, M. Tanaka, K. Tsuruho, K. Okitsu and Y. Maeda, Sonochemical Decomposition of Perfluorooctane Sulfonate and Perfluorooctanoic Acid, *Environ. Sci. Technol.*, 2005, **39**, 3388–3392.

110 Y. Hui, *Mechanisms of Fenton-like Reactions for Reduction of Refractory Compounds*, PhD Dissertation, Washington State University, Pullman, WA, 2001.

111 P. Scotland, K. M. Wyss, Y. Cheng, L. Eddy, J. L. Beckham, J. Sharp, Y. Chung, C. H. Choi, T. Si, B. Wang, J. A. Donoso, B. Deng, Y.-Y. Shen, S. G. Zetterholm, C. Griggs, Y. Han, M. Tomson, M. S. Wong, B. I. Yakobson, Y. Zhao and J. M. Tour, Mineralization of captured perfluorooctanoic acid and perfluorooctane sulfonic acid at zero net cost using flash Joule heating, *Nat. Water*, 2025, **3**, 486–496.

112 B. Gomez-Ruiz, S. Gómez-Lavín, N. Diban, V. Boiteux, A. Colin, X. Dauchy and A. Urtiaga, Efficient electrochemical degradation of poly- and perfluoroalkyl substances (PFASs) from the effluents of an industrial wastewater treatment plant, *Chem. Eng. J.*, 2017, **322**, 196–204.

113 M. H. Lin, D. M. Bulman, C. K. Remucal and B. P. Chaplin, Chlorinated Byproduct Formation during the Electrochemical Advanced Oxidation Process at Magneli Phase Ti$_4$O$_7$ Electrodes, *Environ. Sci. Technol.*, 2020, **54**, 12673–12683.

114 Q. Zhuo, S. Deng, B. Yang, J. Huang, B. Wang, T. Zhang and G. Yu, Degradation of perfluorinated compounds on a boron-doped diamond electrode, *Electrochim. Acta*, 2012, **77**, 17–22.

115 J. Xu, Y. Liu, D. Li, L. Li, Y. Zhang, S. Chen, Q. Wu, P. Wang, C. Zhang and J. Sun, Insights into the electrooxidation of florfenicol by a highly active La-doped Ti$_4$O$_7$ anode, *Sep. Purif. Technol.*, 2022, **291**, 120904.

116 J. Ge, X. Zou, S. Almassi, L. Ji, B. P. Chaplin and A. J. Bard, Electrochemical Production of Si without Generation of CO$_2$ Based on the Use of a Dimensionally Stable Anode in Molten CaCl$_2$, *Angew Chem. Int. Ed. Engl.*, 2019, **58**, 16223–16228.

117 Z. Wang, F. Xiao, X. Shen, D. Zhang, W. Chu, H. Zhao and G. Zhao, Electronic Control of Traditional Iron-Carbon Electrodes to Regulate the Oxygen Reduction Route to Scale Up Water Purification, *Environ. Sci. Technol.*, 2022, **56**, 13740–13750.

118 X. Tan, J. Zhong, C. Fu, H. Dang, Y. Han, P. Král, J. Guo, Z. Yuan, H. Peng, C. Zhang and A. K. Whittaker, Amphiphilic Perfluoropolyether Copolymers for the Effective Removal of Polyfluoroalkyl Substances from Aqueous Environments, *Macromolecules*, 2021, **54**, 3447–3457.

119 G. Pliego, J. A. Zazo, P. Garcia-Muñoz, M. Munoz, J. A. Casas and J. J. Rodriguez, Trends in the Intensification of the Fenton Process for Wastewater Treatment: An Overview, *Crit. Rev. Environ. Sci. Technol.*, 2015, **45**, 2611–2692.

120 J. Xiao, S. Guo, D. Wang and Q. An, Fenton-Like Reaction: Recent Advances and New Trends, *Chemistry*, 2024, **30**, e202304337.

121 A. Babuponnusami and K. Muthukumar, A review on Fenton and improvements to the Fenton process for wastewater treatment, *J. Environ. Chem. Eng.*, 2014, **2**, 557–572.

122 M. Umar, H. A. Aziz and M. S. Yusoff, Trends in the use of Fenton, electro-Fenton and photo-Fenton for the treatment of landfill leachate, *Waste Manage.*, 2010, **30**, 2113–2121.

123 A. Mirzaei, Z. Chen, F. Haghighat and L. Yerushalmi, Removal of pharmaceuticals from water by homo/ heterogonous Fenton-type processes – A review, *Chemosphere*, 2017, **174**, 665–688.

124 R. G. Zepp, B. C. Faust and J. Hoigne, Hydroxyl radical formation in aqueous reactions (pH 3-8) of iron(II) with hydrogen peroxide: the photo-Fenton reaction, *Environ. Sci. Technol.*, 1992, **26**, 313–319.

125 M. Roccamante, I. Salmerón, A. Ruiz, I. Oller and S. Malato, New approaches to solar Advanced Oxidation Processes for elimination of priority substances based on electrooxidation and ozonation at pilot plant scale, *Catal. Today*, 2020, **355**, 844–850.

126 M. E. Demir, G. Chehade, I. Dincer, B. Yuzer and H. Selcuk, Synergistic effects of advanced oxidization reactions in a combination of TiO$_2$ photocatalysis for hydrogen production and wastewater treatment applications, *Int. J. Hydrogen Energy*, 2019, **44**, 23856–23867.